Stochastic Environmental Research and Risk Assessment
https://doi.org/10.1007/s00477-025-03053-6

ORIGINAL PAPER

Space-time blind source separation and linear coregionalization modeling: a critical comparison

Claudia Cappello[1] · **Sandra De Iaco**[1,2] · **Monica Palma**[1,2] · **Klaus Nordhausen**[3]

Accepted: 5 July 2025

Abstract
In many fields of science, multivariate spatio-temporal data can exhibit quite complex dependence structures between the variables and over the domain. Many approaches exist to model such data and usually their starting point is the matrix-valued covariance function (CF). The well-established space-time linear coregionalization model (ST-LCM) and more recently the space-time blind source separation-based model (ST-BSS) can easily support the modeling stage, since they rely on the univariate analysis of latent components. Although they have been developed within distinct backgrounds and some differences between them can be highlighted, they also share various similarities from a theoretical and practical point of view. A critical review of the hypothesis, properties and characteristics of the two approaches is then proposed and a comparison of their performances is provided through a real dataset analysis and a simulation study.

Keywords Space-time covariance function · Multivariate spatio-temporal data · Space-time prediction · Dimension reduction

1 Introduction

Various scientific fields require using appropriate techniques to analyze a dataset characterized by spatial or spatio-temporal structure and referring to multiple correlated variables. Multivariate Geostatistics offers various methods for describing and interpolating the correlation pattern exhibited by the variables being investigated in an accurate and reliable way (Abulkhair et al. 2023). In this context, most of the efforts are aimed at estimating and identifying a model for the matrix-valued CF, which is able to explain the spatial or spatio-temporal direct and cross linear dependence among the variables, as seen in Rouhani and Wackernagel (1990); De Iaco et al. (2003); Berrocal et al. (2010); De Iaco and Posa (2013); Calculli et al. (2015); Ip and Li (2016, 2017a, 2017b); Krupskii and Genton (2017); Otto et al. (2024a), (2024b). Recently, there have also been comprehensive reviews on spatio-temporal covariance modeling, such as those by Chen et al. (2021); Porcu et al. (2021). Morever, a novel multivariate spatio-temporal model, based on the Gneiting family, was recently introduced by Bourotte et al. (2016); Allard et al. (2022); Dörr and Schlather (2023). Nevertheless, the linear coregionalization model (LCM) first proposed for multivariate geostatistical analyses (Journel and Huijbregts 1978; Myers 1995; Wackernagel 2003; Babak and Deutsch 2009; Emery 2010) and successively extended to the spatio-temporal context (ST-LCM) as discussed in Genton and Kleiber (2015); Li et al. (2007); De Iaco et al. (2003, 2005, 2019); Cappello et al. (2022), is a computationally flexible approach widely adopted for various applications (Gneiting at al. 2010; Bevilacqua et al. 2015; De Iaco et al. 2012, 2023, 2025; Cappello et al. 2021; Palma et al. 2023). Through this approach the matrix-valued CF is modeled by linearly combining univariate

✉ Sandra De Iaco
sandra.deiaco@unisalento.it

Claudia Cappello
claudia.cappello@unisalento.it

Monica Palma
monica.palma@unisalento.it

Klaus Nordhausen
klaus.nordhausen@helsinki.fi

[1] DES-Sect. of Mathematics and Statistics, University of Salento, Lecce, Italy

[2] National Center of High Performance Computing, Big Data and Quantum Computing, Bologna, Italy

[3] Department of Mathematics and Statistics, University of Helsinki, Helsinki, Finland

Published online: 12 November 2025

models which are related to latent uncorrelated processes underlying the phenomenon being studied. In this case, the latent uncorrelated components are detected through a joint diagonalization method applied to the covariance matrices computed for distinct lags.

Another recent approach for modeling a multivariate random field has been developed in the framework of blind source separation (BSS), originally introduced for spatial data (Nordhausen et al. 2015; Cabral Pinto et al. 2021; Sipilä et al. 2024, Muehlmann et al. 2025) and more recently extended to spatio-temporal data (ST-BSS) by Muehlmann et al. (2023), where computational advantages have been highlighted. While ST-LCM begins from the perspective of the CF and derives a latent variable model to facilitate covariance estimation, ST-BSS takes the reverse approach: it starts with a latent variable model and focuses on estimating the latent components. This, in turn, implicitly defines the covariance structure and enables its estimation. Both the ST-LCM, based on the covariance matrices' joint diagonalization, and the ST-BSS simplify the multivariate modeling and prediction steps since in both cases the identification of the uncorrelated latent components reduces a multivariate spatio-temporal problem into an univariate context where the latent components are modeled separately. Moreover, the comparison is also consistent since both assume that the multivariate spatio-temporal random field (MSTRF) is obtained by linearly combining uncorrelated random variables, each characterized by a basic CF. Besides these aspects, other interesting similarities and dissimilarities between the two approaches need to be discussed, from both theoretical and practical perspectives. For this reason, the main features of the two methods are delineated in the present contribution and their fitting performances are also highlighted through a real environmental application and a simulation study. Thus, the aim of the paper is to provide not only a critical review of the two methods, namely ST-LCM and ST-BSS, but also to provide useful hints for performing multivariate spatio-temporal analyses for prediction and simulation purposes, since both of them simplify the spatio-temporal multivariate analysis by detecting and modeling the most significant latent components underlying the variables under study. As far as known, in the literature there does not exist a similar contribution which on one hand offers a theoretical and empirical comparison between these two approaches of modeling MSTRFs, and on the other hand discusses their modeling procedures, also through the above-mentioned case studies.

It is worth pointing out that both methodologies rely on the theory of the spatio-temporal random fields. Indeed, given a vector of variables, the related observations recorded at various sampling locations and time points are assumed to be a realization of a MSTRF $\{\mathbf{X}(\mathbf{s},t),(\mathbf{s},t) \in \mathcal{S} \times \mathcal{T} \subseteq \mathbb{R}^d \times \mathbb{R}, d \leq 3\}$, where $\mathbf{X}(\mathbf{s},t) = [X_1(\mathbf{s},t),\ldots,X_p(\mathbf{s},t)]^\top$, $p \geq 2$. By assuming the second-order stationarity, the first order moment of the MSTRF is $\boldsymbol{\mu} = [\mu_1,\ldots,\mu_p]^\top$, where μ_i is the expected value of X_i, $i = 1,\ldots,p$, and the second order moment for any $(\mathbf{s},t)$ and $(\mathbf{s}',t') \in \mathcal{S} \times \mathcal{T}$ whose separation vector is $(\mathbf{h}_s,h_t) \in \mathbb{R}^d \times \mathbb{R}$, with $\mathbf{h}_s = (\mathbf{s}-\mathbf{s}')$ and $h_t = (t-t')$, is $\mathbf{C}(\mathbf{h}_s,h_t) = [C_{ij}(\mathbf{h}_s,h_t)]$, where $= \mathbb{E}[(X_i(\mathbf{s}+\mathbf{h}_s,t+h_t) \cdot X_j(\mathbf{s},t))] - \mu_i\,\mu_j$ is the cross CF for any X_i and X_j, $i,j = 1,\ldots,p$, with $i \neq j$, while for $i = j$, it is the direct CF of X_i. For simplicity, the following notation $C_{ij}(\mathbf{0},0) = \mathbf{Cov}(\mathbf{X}(\mathbf{s},t))$ has been used.

The paper is structured in seven sections. After an accurate explanation of the ST-BSS model (Sect. 2) and the corresponding unmixing matrix functionals and properties, the procedure to select an ST-LCM is detailed (Sect. 3) and the similar and dissimilar features between ST-BSS and ST-LCM are pointed out (Sect. 4). Then, Sect. 5 is devoted to the presentation of a detailed case study, concerning seven agrometeorological indicators, i.e., evapotranspiration level, maximum and minimum temperature, maximum and minimum humidity, wind speed and rainfall, whose weekly data have been measured at some observation points in the Veneto Region (Italy) during the period 2000-2022, and the application of the space-time modeling procedures based on both approaches is discussed in Sect. 5.1. Indexes of fitting accuracy are calculated to compare the performance (in terms of prediction accuracy) of the ST-BSS to the ST-LCM one (Sect. 5.2). In Sect. 6, the findings obtained from the simulation study are presented and a comparative analysis, taking into account different options regarding the quantity of variables and the various scales of variability, is proposed. Finally, conclusions with a discussion on possible future research are reported in Sect. 7.

2 ST-BSS model

BSS has its roots in the signal processing community, initially focusing on independent and identically distributed (iid) data and time series, as highlighted in Hyvärinen et al. (2001); Cichocki and Amari (2002). However, in recent years, it has garnered significant interest in the statistics community (Nordhausen and Oja 2018; Pan et al. 2021), expanding its applications also to spatial data (Nordhausen et al. 2015; Bachoc et al. 2020; Wu et al. 2024). Within the framework of spatial data analysis, it is referred to as Spatial Blind Source Separation (SBSS). More recently, its scope has been extended to irregular spaced space-time data as well (Muehlmann et al. 2023), by introducing the acronym ST-BSS.

The core concept of BSS revolves around the idea that observable data can be interpreted as a mix of hidden processes. The primary objective is to estimate these latent processes solely based on the observable data. While the original motivation stemmed from attributing physical meanings to these latent processes, contemporary research emphasizes that these latent processes are often more interpretable and manageable than the observable data itself.

2.1 ST-BSS model formalism and characteristics

The BSS model formulated for spatio-temporal data by Muehlmann et al. (2023) can be expressed as follows:

$$\mathbf{X}(\mathbf{s},t) = \mathbf{A}\mathbf{Z}(\mathbf{s},t) + \boldsymbol{\mu}, \tag{1}$$

where $\mathbf{X}(\mathbf{s},t)$ represents a p-variate random field, $\mathbf{Z}(\mathbf{s},t)$ comprises second-order stationary and independent components $Z_i(\mathbf{s},t)$, with $i = 1,\dots,p$. The mixing matrix $\mathbf{A}$ is a full-rank $(p \times p)$ matrix, and $\boldsymbol{\mu}$ is a p-dimensional location vector. The goal is then to find an unmixing matrix $\mathbf{W}$ that can recover $\mathbf{Z}(\mathbf{s},t)$ from the observed data $\mathbf{X}(\mathbf{s},t)$ alone, i.e., find a $\mathbf{W}$ such that $\mathbf{W}\left(\mathbf{X}(\mathbf{s},t) - \boldsymbol{\mu}\right) = \mathbf{Z}(\mathbf{s},t)$.

The motivation behind this approach is that, if $\mathbf{Z}(\mathbf{s},t)$ exhibits uncorrelated or independent components, modeling p independent univariate processes is more tractable than dealing with a full p-variate process. This simplification enables researchers to make predictions for each latent process independently and, if necessary, transform them back to the original scale using $\mathbf{W}^{-1}$. This approach has been effectively implemented in a range of settings, such as in multivariate spatial prediction (Muehlmann et al. 2021).

In summary, the ST-BSS workflow can be outlined as follows:

I. Estimate the unmixing matrix $\mathbf{W}$ and the mean $\boldsymbol{\mu}$ to obtain the latent processes $\mathbf{Z}(\mathbf{s},t)$.
II. Model each component of $\mathbf{Z}(\mathbf{s},t)$ univariately.
III. If required, back-transform the quantities of interest to scale of $\mathbf{X}(\mathbf{s},t)$ using $\mathbf{W}^{-1}$ (and $\boldsymbol{\mu}$).

An obvious question that comes up in the framework of ST-BSS is how to estimate the unmixing matrix $\mathbf{W}$ and what additional assumptions are necessary? The assumptions made by Muehlmann et al. (2023) are as follows:

(ST-BSS 1) $\mathbb{E}[\mathbf{Z}(\mathbf{s},t)] = \mathbf{0}$, $\mathbf{Cov}(\mathbf{Z}(\mathbf{s},t)) = \mathbf{I}_p$, where $\mathbf{I}_p$ represents the identity matrix of order p.

(ST-BSS 2) $\mathbf{Cov}(\mathbf{Z}(\mathbf{s},t), \mathbf{Z}(\mathbf{s}',t')) = \mathbb{E}[\mathbf{Z}(\mathbf{s},t)\mathbf{Z}(\mathbf{s}',t')] = \mathbf{D}(\mathbf{h}_s, h_t)$, where $\mathbf{D}(\mathbf{h}_s, h_t)$ is a diagonal matrix. The l-th diagonal element of this matrix corresponds to the covariance of the l-th entry of the latent process $\mathbf{Z}(\mathbf{s},t)$, denoted as $c_l(\mathbf{h}_s, h_t)$.

(ST-BSS 3) The components of $\mathbf{Z}(\mathbf{s},t)$ are independent.

Therefore, assumption (ST-BSS 1) establishes the location and scale of the latent components. The second assumption, (ST-BSS 2), specifies that all components are uncorrelated, both in space and time. Additionally, it asserts that the dependence between different observations relies solely on the spatio-temporal separation distance between them. Assumption (ST-BSS 3) goes beyond uncorrelatedness by requiring independence between the components. The assumption of independence is standard in the BSS literature and enables the subsequent analysis to treat each component separately. This assumption can be motivated as one of two natural ways to generalize the multivariate normal distribution—either by preserving the elliptical shape of the probability contours or by maintaining the independence property of the standard normal case (Nordhausen and Oja 2018). In practice, when dealing with dependent data, as is the case here, the assumption of independence can often be relaxed to uncorrelatedness to achieve identifiability of the latent components. This is, for example, the case in the BSS time series method SOBI (Miettinen et al. 2016).

Consequently, $\mathbf{Z}(\mathbf{s},t)$ exhibits second-order stationarity, which also extends to $\mathbf{X}(\mathbf{s},t)$, resulting in

$$\mathbf{Cov}(\mathbf{X}(\mathbf{s},t), \mathbf{X}(\mathbf{s}',t')) = \mathbf{A}\mathbf{D}(\mathbf{h}_s, h_t)\mathbf{A}^\top, \tag{2}$$

therefore it is also easy to see that the space-time covariance matrix of $\mathbf{X}(\mathbf{s},t)$ is symmetric and usually not separable.

Still, the conditions (ST-BSS 1) - (ST-BSS 3) do not specify the model completely as for a given pair of $(\mathbf{A}, \mathbf{Z}(\mathbf{s},t))$, the pair $(\mathbf{APJ}, \mathbf{JP}^\top\mathbf{Z}(\mathbf{s},t))$ leads to the same observable $\mathbf{X}(\mathbf{s},t)$ where the two latent fields $\mathbf{Z}(\mathbf{s},t)$ and $\mathbf{JP}^\top\mathbf{Z}(\mathbf{s},t)$ do not violate conditions (ST-BSS 1)-(ST-BSS 3). This holds true for any $\mathbf{P} \in \mathcal{P}^p$ and $\mathbf{J} \in \mathcal{J}^p$ where $\mathcal{P}^p$ is the set of all $(p \times p)$ permutation matrices and $\mathcal{J}^p$ is the set of all sign-change matrices, i.e., diagonal matrices with diagonal elements ± 1. Hence, the latent field (or equivalently the mixing matrix) is only identifiable up to permutation and sign (of its rows). Thus $\mathbf{W}$ is equivalent to $\mathbf{A}^{-1}$ up to sign changes and order of the rows. This identifiability issue, which applies to all BSS approaches, is usually not considered a problem, in practice. To guarantee the parameters' identifiability, condition (ST-BSS 2) must be substituted with a slightly stringent assumption, which varies based on the used estimator, as discussed in the following for the two estimators considered here.

Despite these sources of indeterminacy, it is noteworthy that the ST-BSS model simplifies the second-order spatio-temporal dependence significantly. This simplification arises because the second-order dependence structure is entirely defined by the $(p \times p)$ matrix $\mathbf{A}$ and p univariate

stationary spatio-temporal CFs. This stands in stark contrast to the scenario where no assumptions about $\mathbf{X}(\mathbf{s},t)$ are made, which would require modeling p covariances and $p(p-1)/2$ cross CFs.

2.2 Unmixing matrix functionals and properties

Muehlmann et al. (2023) suggested two types of estimators for the unmixing matrix $\mathbf{W}$. Both types are based on local autocovariance matrices (LACF) which are defined for n space-time locations as

$$\begin{aligned}&\mathbf{LACF}_f(\mathbf{X}(\mathbf{s},t))\\&= \tfrac{1}{nF_{n,f}} \sum_{i,j=1}^{n} f(\mathbf{s}_i-\mathbf{s}_j,t_i-t_j)\mathbb{E}\left((\mathbf{X}(\mathbf{s}_i,t_i)-\boldsymbol{\mu})(\mathbf{X}(\mathbf{s}_j,t_j)-\boldsymbol{\mu})^\top\right)\end{aligned} \tag{3}$$

where the spatio-temporal kernel function $f:\mathbb{R}^{d+1}\to\mathbb{R}$ defines the locality and

$$F_{n,f}^2 = \frac{1}{n}\sum_{i,j=1}^{n} f^2(\mathbf{s}_i-\mathbf{s}_j,t_i-t_j) \tag{4}$$

is a normalizing constant for the denseness in the locality. To avoid the necessity to introduce a metric which combines time and space, Muehlmann et al. (2023) suggested to measure locality via the following kernel functions

Ball kernel $f_b(\mathbf{h}_s,h_t;r_s,r_t) = I(\|\mathbf{h}_s\|\le r_s)I(|h_t|\le r_t)$, with $r_s\ge 0, r_t\ge 0$ and I denotes the indicator function.

Ring kernel $f_r(\mathbf{h}_s,h_t;r_{s_0},r_{s_1},r_{t_0},r_{t_1}) = I(r_{s_1}<\|\mathbf{h}_s\|\le r_{s_0})I(r_{t_1}<|h_t|\le r_{t_0}))$, with $r_{s_0}>r_{s_1}\ge 0, r_{t_0}>r_{t_1}\ge 0$.

Gauss kernel $f_g(\mathbf{h}_s,h_t;r_s,r_t,\alpha) = \exp(-0.5\ \Phi^{-1}(1-\alpha)^2[(\|\mathbf{h}_s\|/r_s)^2+(|h_t|/r_t)^2])$, where $\Phi^{-1}(1-\alpha)$ is the $(1-\alpha)$ 100% quantile of the standard Normal distribution and $r_s\ge 0,\ r_t\ge 0$. Muehlmann et al. (2023) recommended using $\alpha = 0.05$.

Note that some other kernels in a pure spatial context were suggested in Muehlmann et al. (2024) and could also be used here for the spatial part of the kernels.Muehlmann et al. (2023) proposed then two estimators of the unmixing where the main idea is to jointly diagonalize the covariance matrix and one or more different LACFs. When two matrices are involved the estimator is called stAMUSE. For a chosen spatio-temporal kernel f, the stAMUSE unmixing matrix $\mathbf{W}=\mathbf{W}(\mathbf{X}(\mathbf{s},t))$ simultaneous diagonalizes $\mathbf{Cov}$ and $\mathbf{LACF}$ as follows:

$$\mathbf{W}\,\mathbf{Cov}(\mathbf{X}(\mathbf{s},t))\mathbf{W}^\top = \mathbf{I}_p \quad\text{and}\quad \mathbf{W}\,\mathbf{LACF}_f(\mathbf{X}(\mathbf{s},t))\mathbf{W}^\top = \mathbf{D}_f, \tag{5}$$

where $\mathbf{D}_f$ is a diagonal matrix whose diagonal entries are arranged in decreasing order. Thus, stAMUSE can be determined through a decomposition into generalized eigenvalues and eigenvectors where $\mathbf{D}_f$ then contains the corresponding generalized eigenvalues. Therefore it is also obvious that stAMUSE is well-defined if the diagonal elements of $\mathbf{D}_f$ are all distinct. Therefore it requires that (i) all latent random fields must have a different space-time covariance matrix and (ii) the kernel f must be chosen wisely.

To avoid making a single choice, the alternative is not to diagonalize two matrices but more than two. The estimator stSOBI (Muehlmann et al. 2023) requires $K>1$ different spatio-temporal kernel functions $f_1,\dots,f_K$ and is then defined as the matrix $\mathbf{W}$ which maximizes

$$\sum_{k=1}^{K} ||\operatorname{diag}(\mathbf{W}\,\mathbf{LACF}_{f_k}(\mathbf{X}(\mathbf{s},t))\mathbf{W}^\top)||^2 \tag{6}$$

under the constraint that $\mathbf{W}\,\mathbf{Cov}(\mathbf{X}(\mathbf{s},t))\mathbf{W}^\top=\mathbf{I}_p$, where $\operatorname{diag}(\cdot)$ extracts the diagonal elements and $||\cdot||$ gives the Frobenius norm. There are many algorithms to solve such joint diagonalization problems; the one based on Jacobi rotations (Clarkson 1988) has been used in this paper. The advantage of stSOBI over stAMUSE is that it is now sufficient that there exists $k\in\{1,\dots,K\}$ such that $(\mathbf{LACF}_{f_k}(\mathbf{Z}(\mathbf{s},t)))_{ii}\neq(\mathbf{LACF}_{f_k}(\mathbf{Z}(\mathbf{s},t)))_{jj}$, for all $i,j=1,\dots,p$ and $i\neq j$.

Let $\mathbf{w}_i$ denote the i-th row of $\mathbf{W}$, then the squared pseudo-eigenvalues

$$\begin{aligned}&\lambda_{i,k}^2 = (\mathbf{w}_i^\top\mathbf{LACF}_{f_k}(\mathbf{X}(\mathbf{s},t))\mathbf{w}_i)^2\\&\text{for } i=1,\dots,p \text{ and } k=1,\dots,K,\end{aligned} \tag{7}$$

can be interpreted as a measure of spatio-temporal dependence and often the components are ordered such that $\sum_{k=1}^K\lambda_{i,k}^2$ is in decreasing order.

To acquire the finite sample estimations of stAMUSE and stSOBI, the corresponding kernels need to be chosen, and then the corresponding sample versions of $\mathbf{Cov}(\cdot)$ and $\mathbf{LACF}_f(\cdot)$ are jointly diagonalized. Joint diagonalization of two or more matrices has a long tradition in BSS; see, among others, Nordhausen and Ruiz-Gazen (2022) and Tang et al. (2005) for an overview. AMUSE and SOBI were actually introduced in a time series setting, and it is well-known in that framework (Miettinen et al. 2012, 2016) that it is not necessary that the latent components are independent. Hence the assumption (ST-BSS 3) is actually not needed and stAMUSE and stSOBI work also when the latent components are only uncorrelated. More important is that the spectra of the components differ sufficiently and the task of

the user is to select lags in such a way that the eigenvalues of $\mathbf{LACF}_f(\mathbf{Z}(\mathbf{s},t))$ are as distinct as possible. This lag-selection is still an open issue and is usually based on subject knowledge paired with exploratory data analysis. Some visual analytic approaches are discussed, for example, in the pure temporal and pure spatial case in Piccolotto et al. (2022a); Cappello et al. (2024); Piccolotto et al. (2022b) and similar tools should be developed still for ST-BSS. The current approach of ST-BSS assumes p latent fields; often however it is assumed that only a few of them are of interest. Different noise models in the temporal and spatial case are discussed in Nordhausen and Virta (2019); Nordhausen et al. (2022); Muehlmann et al. (2024) where for example it is assumed that noise components are white noise. The aforementioned references give tools to determine the number of interesting components for the pure spatial or pure temporal settings, which are again still missing for ST-BSS. The (pseudo)-eigenvalues of stAMUSE and stSOBI provide however a good starting point to evaluate if the components contain any serial dependence or not.

3 The ST-LCM and the selection procedure

A modeling approach based on an ST-LCM, as in its first introduction by De Iaco et al. (2003), is widely adopted in the literature for many space-time multivariate geostatistical applications, since it is flexible enough from a computational point of view, as highlighted in Cappello et al. (2022). In the following, a review of the ST-LCM is given and the modeling procedure is recalled.

3.1 ST-LCM background

The ST-LCM is built by linearly combining L ($L \leq p$) basic scalar CFs; specifically, the matrix $\mathbf{C}$ is modeled as follows:

$$\mathbf{C}(\mathbf{h}_s, h_t) = \sum_{l=1}^{L} \mathbf{B}_l \; c_l(\mathbf{h}_s, h_t), \tag{8}$$

where $c_l(\mathbf{h}_s, h_t)$ represent the above-mentioned basic scalar covariances related to the hidden variables of the random field $\mathbf{X}$ and $\mathbf{B}_l = [b_{ij}^l], l = 1, \ldots, L$, are matrices of dimension $(p \times p)$, called coregionalization matrices, which must be positive definite for the admissibility of model (8).

Note that the structure of the above covariance model can be derived from the assumption that each component of $\mathbf{X}(\mathbf{s},t)$ is assumed to be constructed as a linear combination of uncorrelated second-order stationary random functions, e.g. $\mathbf{Y}_l(\mathbf{s},t) = [Y_l^1(\mathbf{s},t), Y_l^2(\mathbf{s},t), \ldots, Y_l^p(\mathbf{s},t)]^\top, \; l = 1, \ldots, L$. Then

$$\mathbf{X}(\mathbf{s},t) = \sum_{l=1}^{L} \mathbf{A}_l \; \mathbf{Y}_l(\mathbf{s},t) + \boldsymbol{\mu}, \tag{9}$$

where $\mathbf{A}_l$ is a $(p \times p)$ coefficient matrix for each $l = 1, \ldots, L$ and $\boldsymbol{\mu} = [\mu_1, \ldots, \mu_p]^\top$ is the vector of the expected values of the random fields X_i. In particular, the random fields Y_l^i, $i = 1, \ldots, p, l = 1, \ldots, L$, are such that $\mathbb{E}[Y_l^i(\mathbf{s},t)] = 0$ and

$$Cov[Y_l^i(\mathbf{s},t), Y_l^i(\mathbf{s}+\mathbf{h}_s, t+h_t)] = c_l(\mathbf{h}_s, h_t),$$
$$Cov[Y_l^i(\mathbf{s},t), Y_k^j(\mathbf{s}+\mathbf{h}_s, t+h_t)] = 0, \quad i \neq j, l \neq k.$$

More specifically, the above model can be explained by clarifying that

- each random field X_i of the MSTRF $\mathbf{X}$ is assumed to be decomposed into the sum of the spatially and temporally uncorrelated factors $\{X_l^i(\mathbf{s},t); l = 1, \ldots, L\}$, that is

$$X_i(\mathbf{s},t) = \sum_{l=1}^{L} X_l^i(\mathbf{s},t) + \mu_i,$$

where $\mathbb{E}[X_i(\mathbf{s},t)] = \mu_i, \mathbb{E}[X_l^i(\mathbf{s},t)] = 0$,
$Cov[X_l^i(\mathbf{s},t), X_l^j(\mathbf{s}+\mathbf{h}_s, t+h_t)]$
$= \mathbb{E}[X_l^i(\mathbf{s},t)\, X_l^j(\mathbf{s}+\mathbf{h}_s, t+h_t)] = C_{ij}^l(\mathbf{h}_s, h_t)$ and
$Cov[X_l^i(\mathbf{s},t), X_k^j(\mathbf{s}+\mathbf{h}_s, t+h_t)] = 0, l \neq k$;

- each spatio-temporal component X_l^i is defined as a combination of uncorrelated factors Y_l^j, $j = 1, \ldots, p$, with coefficients a_{jl}^i,

$$X_l^i(\mathbf{s},t) = \sum_{j=1}^{p} a_{jl}^i Y_l^j(\mathbf{s},t).$$

Thus, from the above two points, it results the model in (9), which can be explicitly written as

$$X_i(\mathbf{s},t) = \sum_{l=1}^{L} \sum_{j=1}^{p} a_{jl}^i Y_l^j(\mathbf{s},t) + \mu_i.$$

The cross CFs $C_{ij}^l(\mathbf{h}_s, h_t)$, associated to the factors $X_l^i(\mathbf{s},t)$, are linked to the CF $c_l(\mathbf{h}_s, h_t)$ through the coefficient of proportionality b_{ij}^l, that is $C_{ij}^l(\mathbf{h}_s, h_t) = b_{ij}^l c_l(\mathbf{h}_s, h_t)$, thus

$$C_{ij}(\mathbf{h}_s, h_t) = \sum_{l=1}^{L} C_{ij}^l(\mathbf{h}_s, h_t) = \sum_{l=1}^{L} b_{ij}^l c_l(\mathbf{h}_s, h_t). \tag{10}$$

It is also worth underlining that, in practice once the matrices $\mathbf{B}_l$ are determined from the empirical multivariate CF, they can be decomposed to obtain the matrices $\mathbf{A}_l$, that is

$\mathbf{B}_l = \mathbf{A}_l \mathbf{A}_l^\top$, $\mathbf{A}_l = [a_{kl}^i]$. This factorization can be computed through the eigenvalue decomposition of each coregionalization matrix.

For details, the readers can refer to Myers (1995); Wackernagel (2003) and De Iaco et al. (2005).

Remarks

- The components $c_l(\mathbf{h}_s, h_t)$ are called "basic" since their value at zero is usually set to be one; thus, they are also denoted with $\rho_l(\mathbf{h}_s, h_t)$ to indicate the correlation function.
- In the geostatistical literature, a special case of ST-LCM obtained when $L = 1$ is the so-called intrinsic model. In particular, the CF matrix which explains the relationship among the variables at the spatio-temporal lag $(\mathbf{h}_s, h_t)$ is defined as the multiplication of the variance-covariance matrix $\mathbf{B}$ with a spatio-temporal univariate CF $c(\mathbf{h}_s, h_t)$ which is the same for all variables and measures their relations between the points in space-time, that is:

$$\mathbf{C}(\mathbf{h}_s, h_t) = \mathbf{B}\, c(\mathbf{h}_s, h_t). \tag{11}$$

The property of this model is that the correlation ρ_{ij} between two variables X_i and X_j does not depend on the spatio-temporal lag:

$$\frac{C_{ij}(\mathbf{h}_s, h_t)}{\sqrt{C_{ii}(\mathbf{h}_s, h_t) C_{jj}(\mathbf{h}_s, h_t)}} = \frac{b_{ij} c(\mathbf{h}_s, h_t)}{\sqrt{b_{ii} c(\mathbf{h}_s, h_t) b_{jj} c(\mathbf{h}_s, h_t)}} = \frac{b_{ij}}{\sqrt{b_{ii} b_{jj}}} = \rho_{ij},$$

which implies that the direct and cross CFs are all proportional to a same basic spatio-temporal correlation function: $C_{ij}(\mathbf{h}_s, h_t) = b_{ij} c(\mathbf{h}_s, h_t)$. In this case, the equation (9) reduces to $\mathbf{X}(\mathbf{s}, t) = \mathbf{A}\, \mathbf{Y}(\mathbf{s}, t) + \boldsymbol{\mu}$, which analytically corresponds to the ST-BSS model.

3.2 Modeling steps

The model in (8) is fitted following the outlined steps below:

I. Selection of the uncorrelated components, defined by jointly diagonalizing the sample covariance matrices, and computation of the empirical basic CFs;
II. Modeling the empirical basic CFs by adopting classes of models which are adequate in accordance to the empirical features of each basic component;
III. Calculation of positive definite matrices of coregionalization.

Step I starts with the computation of the symmetric $(p \times p)$ matrix $\widehat{\mathbf{C}}(\mathbf{h}_s, h_t)_k = [\widehat{C}_{ij}(\mathbf{h}_s, h_t)_k]$ obtained, for each lag $(\mathbf{h}_s, h_t)_k$, with $k = 1, \ldots, K$, by taking into account all observations at any pair of sample points $(\mathbf{s}, t)$ and $(\mathbf{s}', t')$ such that the separation lag is $(\mathbf{h}_s, h_t)_k$ (Wackernagel 2003). Then, the sample covariance matrices calculated at distinct space-time lags are jointly diagonalized with the aim of detecting the basic components:

$$\boldsymbol{\Psi}\, \widehat{\boldsymbol{C}}(\mathbf{h}_s, h_t)_k\, \boldsymbol{\Psi}^\top = \boldsymbol{\Lambda}(\mathbf{h}_s, h_t)_k, \qquad k = 1, \ldots, K, \tag{12}$$

where $\boldsymbol{\Psi}$ is a $(p \times p)$ orthogonal matrix and $\boldsymbol{\Lambda}_k$ are the diagonal $(p \times p)$ matrices. Joint diagonalization with respect to the lags implies that $\boldsymbol{\Psi}$ is independent of the lags. There are many algorithms performing joint diagonalization, see Illner et al. (2015) for a comprehensive summary. For the purpose of the joint diagonalization, the algorithm based on Jacobi rotations (Cardoso and Souloumiac 1996) will be adopted, which is for example available in the R package JADE (Miettinen et al. 2017). The estimates of c_l $(l = 1, \ldots, p)$, denoted with $\hat{c}_l$, for the K spatio-temporal lags are achieved by retrieving all the diagonal elements from the K diagonal matrices $\boldsymbol{\Lambda}(\mathbf{h}_s, h_t)_k$, $k = 1, \ldots, K$ (Myers 1995, Xie and Myers 1995). Then, only the $L \leq p$ basic components $\widehat{c}_l, l = 1, \ldots, L$, which exhibit distinct spatio-temporal scales of variability (corresponding to the lag where the surface decays) are selected. Then, they are used in the second step, where they are modeled.

Finally (step III), the matrices $\mathbf{B}_l$, $l = 1, \ldots, L$, of the model in (8) are estimated. Starting from the $p(p+1)/2$ covariances $\widehat{C}_{ij}(\mathbf{h}_s, h_t)$, $i, j = 1, \ldots, p$, the elements b_{ij}^l of $\mathbf{B}_l, l = 1, \ldots, L$, are equal to the ratio between the contributions of $\widehat{C}_{ij}$ at the l-th scale of variability, and $[c_l(\mathbf{0}, 0)]$, i.e.,

$$b_{ij}^l = \frac{[\widehat{C}_{ij}(\mathbf{h}_s, h_t)_{l-1}] - [\widehat{C}_{ij}(\mathbf{h}_s, h_t)_l]}{[c_l(\mathbf{0}, 0)]}, \qquad l = 1, \ldots, L, \tag{13}$$

where $\widehat{C}_{ij}(\mathbf{h}_s, h_t)_0 = \widehat{C}_{ij}(\mathbf{0}, 0)$, with $i, j = 1, \ldots, p$, $i \leq j$.

The admissibility condition for $\mathbf{B}_l, l = 1, \ldots, L$, namely their positive definiteness, is verified in the presence of non-negative eigenvalues. Then, by spectral decomposition of these matrices, $\mathbf{B}_l = \mathbf{V}_l \boldsymbol{\Lambda}_l \mathbf{V}_l^\top$, $l = 1, \ldots, L$, with their eigenvector matrix $\mathbf{V}_l$ and diagonal matrix of the eigenvalues $\boldsymbol{\Lambda}_l$, it suffices to check if any of the eigenvalues are negative, and replace them with zero. In this way, the following transformed matrix $\mathbf{B}_l'$ is obtained

$$\mathbf{B}_l' = \mathbf{V}_l \boldsymbol{\Lambda}_l' \mathbf{V}_l^\top, \qquad l = 1, \ldots, L, \tag{14}$$

where the diagonal matrix of the eigenvalues $\boldsymbol{\Lambda}_l'$ is changed with respect to the original $\boldsymbol{\Lambda}_l$ since zeros replace the negative eigenvalues.

Remarks

- Given the $(p \times p)$ matrix $\boldsymbol{\Psi}$, the components obtained as a matrix multiplication between the $(n \times p)$ data matrix $\mathbf{x}$ and $\boldsymbol{\Psi}$, that is $\tilde{\mathbf{y}} = \mathbf{x}\boldsymbol{\Psi}$, are such that their CFs allow the estimation of the basic components $c_l, l = 1, \ldots, L$. In other terms, given the following model $\mathbf{X}'(\mathbf{s}, t) = \mathbf{A}' \tilde{\mathbf{Y}}(\mathbf{s}, t) + \boldsymbol{\mu}$, where the matrices of coefficients $\mathbf{A}'_j = [a^i_{jl}]$ are such that $\mathbf{A}'_1 = \mathbf{A}'_2 = \ldots = \mathbf{A}'_j = \ldots = \mathbf{A}'_p = \mathbf{A}'$, and

$$\tilde{\mathbf{Y}}(\mathbf{s}, t) = \left[\sum_{i=1}^{p} Y^i_1(\mathbf{s}, t), \ldots, \sum_{i=1}^{p} Y^i_l(\mathbf{s}, t), \ldots, \sum_{i=1}^{m} Y^i_p(\mathbf{s}, t)\right]^\top . \quad (15)$$

  It is important to note that $\mathbf{X}'$ is characterized by the same covariance structure of (8), since $\mathbf{Cov}(\tilde{\mathbf{Y}}(\mathbf{s}, t), \tilde{\mathbf{Y}}(\mathbf{s} + \mathbf{h}_s, t + h_t)) = \mathbf{D}(\mathbf{h}_s, h_t)$, where $\mathbf{D}(\mathbf{h}_s, h_t)$ is a diagonal matrix whose diagonal entries are the covariances $c_l(\mathbf{h}_s, h_t), l = 1, \ldots, p$.
- If the magnitude of the study variables differs, the ST-LCM fitting procedure will be developed by jointly diagonalizing the covariance matrices computed for the standardized variables.

Table 1 Similarities and dissimilarities between ST-LCM and ST-BSS

	ST-LCM	ST-BSS
1. Introduced in	De Iaco et al. (2003, 2013)	Muehlmann et al. (2023)
2. Origins	Mining Geostatistics	Signal processing
3. Initial objective	Estimation of coregionalization matrices	Estimation of the latent components
4. Model for the MSTRF $\mathbf{X}$	Linear	Linear
5. Stationarity	Second-order	Second-order
6. Equivariance	Orthogonal equivariant	Affine equivariant
7. Dependence among variables	Specified by $L(p \times p)$ coregionalization matrices and L basic CFs	Specified by a $(p \times p)$ mixing matrix and p CFs
8. Properties of covariance matrix of $\mathbf{X}$	Symmetric, non-separable	Symmetric, non-separable
9. Latent components	Uncorrelated	Independent (uncorrelated)
10. Covariance model of latent components	Non-parametric, but should reflect different spatio-temporal scales	Non-parametric, but should be different between the components
11. Parameters to estimate	L positive definite coregionalization matrices, L latent CFs	Full rank unmixing matrix
12. Dimension reduction	In-built as $L \leq p$	Optional

4 Similarities and dissimilarities

In this section, backgrounds, hypotheses, properties and characteristics of the two approaches have been discussed, thus, similarities and dissimilarities have been clarified and summarized in Table 1.

The extension of the LCM and BSS from space to space-time dates back to the early years of the new century for the former (De Iaco et al. 2003) and to the beginning of 2020 for the latter (Muehlmann et al. 2023); however, it is worth pointing out that they were developed within different scientific communities (features 1. and 2.). Indeed, the LCM originates from mining Geostatistics (Journel and Huijbregts 1978), while BSS comes from the field of signal processing (Jutten and Taleb 2000).

ST-LCM and ST-BSS diverge considerably in the initial setup and objectives (feature 3.). In ST-LCM, the structure of the space-time covariance matrix is predefined, with the primary objective being the estimation of the coregionalization matrices (in its widest sense, the covariance matrix). During the estimation, as a byproduct, uncorrelated latent components (feature 9. for ST-LCM) can be obtained which represent the predominant scales of space-time dependencies. Conversely, in ST-BSS, the starting point is the assumption of latent components, with the observed data representing a linear mixture of these components. The primary aim here is to estimate these latent components and the unmixing matrix. However, due to the assumptions regarding the latent components and linear mixing, the specification of the space-time covariance matrix is indirectly determined. While Muehlmann et al. (2023) stipulate the independence of latent components (feature 9. for ST-BSS), this requirement is not necessary for identifiability, as only uncorrelatedness is required.

As a consequence, for the ST-BSS the dependence among variables is specified by a $(p \times p)$ mixing matrix and p CFs associated to the p latent components; for the ST-LCM, it is determined by L $(p \times p)$ coregionalization matrices and L basic CFs, from which the p direct CFs of the variables under study and the associated $p(p-1)/2$ symmetric cross CFs are modeled (feature 7.). Regarding other properties, differently from the ST-LCM which is orthogonal equivalent, i.e., invariant under rotation, the ST-BSS is affine equivariant, i.e., if $\mathbf{X}(\mathbf{s}, t)$ is affine transformed by $\mathbf{X}'(\mathbf{s}, t) = \mathbf{M}\mathbf{X}(\mathbf{s}, t) + \mathbf{a}$, where $\mathbf{M}$ is any invertible $(p \times p)$ matrix and $\mathbf{a} \in \mathbb{R}^p$ is any vector, then the unmixing matrix functional $\mathbf{W}(\mathbf{X}'(\mathbf{s}, t))$ should equal $\mathbf{W}(\mathbf{X}'(\mathbf{s}, t))\mathbf{M}^{-1}$ up to permutation and sign (feature 6.). The unmixing matrix's affine equivariance ensures that the estimation is independent by the specific mixing method.

Despite the above mentioned basic divergences, the two methodologies share various similarities, such as the

second-order stationarity (feature 5.) of the MSTRF $\mathbf{X}$, the linearity of its model (feature 4.) and the properties of the covariance matrix of $\mathbf{X}$ (feature 8.), since both methods assume symmetry and non-separability conditions for the covariance matrix of the MSTRF $\mathbf{X}$.

In particular, note that the cross CFs are symmetric if they are invariant with respect to the exchange of the variables or equivalently to the sign of the spatio-temporal lag vector, i.e.,

$$C_{ij}(\mathbf{h}_s, h_t) = C_{ij}(-\mathbf{h}_s, -h_t), \qquad i, j = 1, 2, \ldots, p,\ i \neq j. \tag{16}$$

In addition, the full symmetry condition of the cross CFs occurs if

$$C_{ij}(\mathbf{h}_s, h_t) = C_{ij}(\mathbf{h}_s, -h_t), \qquad i, j = 1, 2, \ldots, p,\ i \neq j. \tag{17}$$

Under the condition (16), strictly positive definite covariance models, discussed in De Iaco and Posa (2018) and De Iaco et al. (2019), can be adopted for the basic structures c_l in (8).

The non-separability of the covariance matrix of $\mathbf{X}$ is satisfied if the changes of the cross-covariances, with respect to the changes of the vector $(\mathbf{h}_s, h_t)$, do not depend on the pair variables X_i, X_j, or in other terms when the following condition of separability is not respected:

$$C_{ij}(\mathbf{h}_s, h_t) = \rho(\mathbf{h}_s, h_t)\, a_{ij}, \qquad i, j = 1, 2, \ldots, p, \tag{18}$$

where a_{ij} are the elements of a $(p \times p)$ positive definite matrix and ρ is a spatio-temporal correlation function. Essentially, the separability condition is satisfied for the intrinsic coregionalization model, obtained from (8) when $L = 1$.

It is worth pointing out that for both methodologies, a non-parametric modeling is adopted for the covariance structure of each latent component, where the basic models c_l of the ST-LCM reflect different spatio-temporal scales, while for the ST-BSS they have to be simply different between the components (feature 10.). These methodologies also share the characteristic that the smoothness of any component of the MSTRF is that of the roughest underlying univariate random field, whose covariance model is an infinitesimal of lower order with respect to the other components of the linear combination (2) or (10).

Moreover, for the modeling aim, a suitable model class must be fitted to each latent component based on some specific characteristics, such as full symmetry ($c_l(\mathbf{h}_s, h_t) = c_l(\mathbf{h}_s, -h_t) = c_l(-\mathbf{h}_s, h_t)$) and separability ($c_l(\mathbf{h}_s, h_t) = c_l(\mathbf{h}_s) c_l(h_t)/c_l(\mathbf{0}, 0)$), which the sample covariance surfaces may show. Note that these are additional properties of the CFs (referred to univariate random fields), which can be useful in this context to describe the spatio-temporal correlation of the latent components, but have not to be confused with the conditions in (16) and (18), stated for the cross-covariance of a MSTRF.

If the separability assumption of the basic component c_l is not likely, then the type of non-separability can be studied through the computation of the sample non-separability ratios, as in De Iaco and Posa (2013):

$$\widehat{r}_l(\mathbf{h}_s, h_t) = \widehat{c}_l(\mathbf{0}, 0) \frac{\widehat{c}_l(\mathbf{h}_s, h_t)}{\widehat{c}_l(\mathbf{h}_s, 0)\widehat{c}_l(\mathbf{0}, h_t)}, \qquad l = 1, \ldots, L, \tag{19}$$

where $L \leq p$ for ST-LCM and $L = p$ for ST-BSS. According to the values of the above mentioned index, uniform positive (negative) non-separability occurs if the ratios in (19) are much greater (lower) than 1 for the fixed lags; or alternatively, non uniform non-separability occurs in all other cases.

The box-plots representation of ratios in (19), grouped by spatial and temporal lags, help the researcher to easily identify the type of non-separability for each basic component. However, in Cappello et al. (2022), some statistical tests were also proposed to determine the statistical significance of the hypotheses on the above mentioned characteristics.

Moreover, it is essential to specify that during the modeling step, the parameters to estimate regard the full rank unmixing matrix for the ST-BSS, while they concern the L positive definite coregionalization matrices and the latent covariance models for the ST-LCM (feature 11.). Nevertheless, in the case that modeling is not the only objective of the analysis, but also prediction purposes have to be pursued, the parameters of the latent covariance models have to be determined even for the ST-BSS. Thus, the sufficient condition for the admissibility of the ST-LCM, implies that if a cross-covariance $C_{ij}(\mathbf{h}_s, h_t)$ discloses two or more nested structures with ranges equal to $a_1, a_2, \ldots$, the same structures have to also appear on the corresponding direct CFs $C_{ii}(\mathbf{h}_s, h_t)$ and $C_{jj}(\mathbf{h}_s, h_t)$; furthermore, a structure may characterize the direct CFs without being included in the cross-covariances. For the ST-BSS, this condition is also ensured from the requirement that $\mathbf{A}$ must be a full rank matrix.

As a consequence, one could argue that both ST-LCM and ST-BSS impart structure to the space-time covariance matrix and yield latent (at least uncorrelated) components that can subsequently be utilized for multivariate data modeling. In particular, regarding the multivariate modeling, the ST-LCM includes the idea of selecting $L \leq p$ latent components, which describe the scales of variability, while for the ST-BSS it is just optional and can be further investigated in the future (feature 12.).

To exemplify the modeling of multivariate space-time data using both approaches, we present a detailed case study describing each modeling step, in the following section. This case study aims to evaluate potential differences in results when using both methods for prediction.

5 Case study

In this case study, the most relevant agrometeorological variables recorded by the Agency for Environmental Prevention and Protection of Veneto region (https://www.arpa.veneto.it/bollettini/storico) have been analyzed. In particular, the following variables have been considered: evapotranspiration levels (ET_0) in *mm*, maximum and minimum air temperature (indicated, respectively, with T_M and T_m) both expressed in $°C$, percentage of maximum and minimum relative humidity (denoted, respectively, with H_M and H_m), wind speed (*WS*) in *m*/*s* and total rainfall (*R*) in *mm*. The study dataset consists of weekly averages recorded for ET_0, T_M, T_m, H_M, H_m and *WS*, as well as of total weekly *R*, taken at 72 monitoring stations spread-out over the Veneto region (Fig. 1) in a 23-year span, that is from the 1st week in 2000 to the 14th week in 2022.

The Veneto region, located between the central European continental area and the Mediterranean one, is extended for about 18,400 *kmq* and represents the eighth largest region among the 20 Italian regions. Almost all the territory is covered by the Venetian Plain which is characterized by very intensive agricultural production, essentially based on wide vineyards from which fine wines are obtained and exported all over the world. In this context, knowing the levels of evapotranspiration, as well as the meteo-climatic conditions, is crucial to determine and plan the amount of water to be given to crops through the fields irrigation. Moreover, ET_0 is one of the climatic parameters that holds significant importance in planning the agricultural production for the efficient use of water resources. Therefore, investigating on the interrelationships among the above-mentioned variables and their joint behavior in space-time could be strategic for the arrangement of possible interventions in the region, especially in areas with massive agricultural land use, such as in the Venetian Plain (De Iaco et al. 2019).

For the aim of this paper, the present case study has been developed as follows. After an exploratory analysis showing the main features of the investigated variables,

a) the hidden spatio-temporal components underlying the environmental phenomenon, will be identified through the two previously discussed approaches, i.e., ST-BSS and ST-LCM; successively, the found components will be modeled with the most suitable models of space-time covariance, and the adequacy of the fitted models will be evaluated;
b) the ST-BSS model and the ST-LCM fitted to the study dataset will be compared in terms of predictive performances; more specifically, the ET_0 levels will be estimated by using the two fitted models and the resulting prediction errors will be compared to highlight the predictive abilities of the two methods (ST-BSS versus ST-LCM).

As a preliminary exploratory analysis, various basic statistical tools have been applied on the observed data.

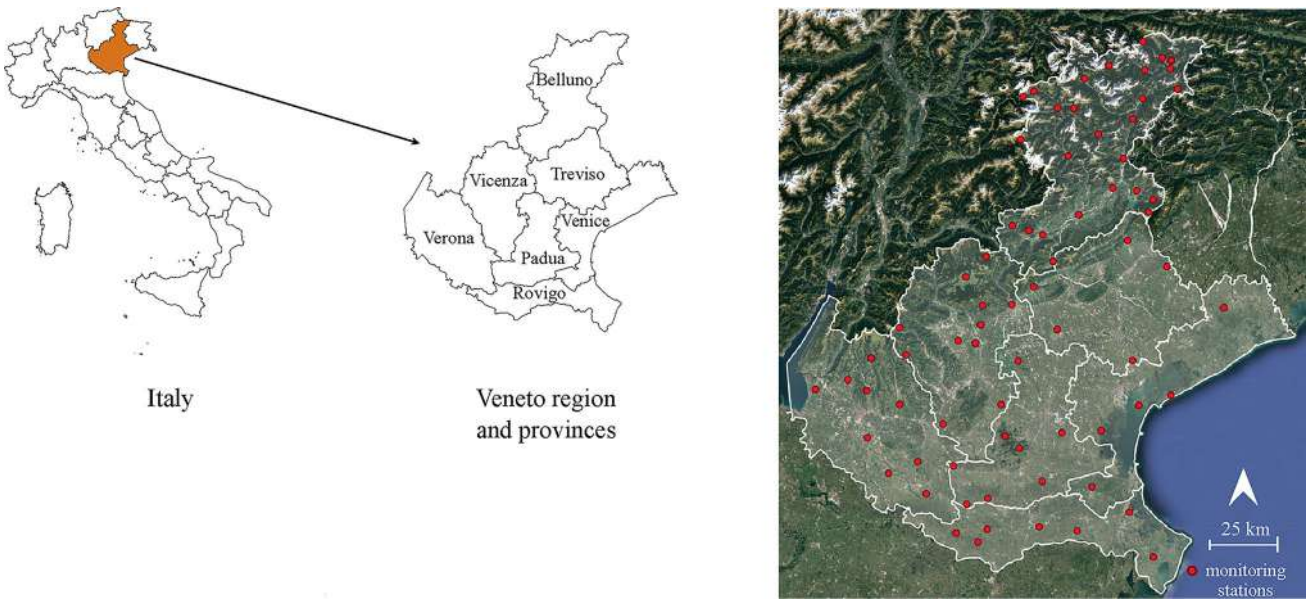

Fig. 1 Location map of the 72 agrometeorological stations in Veneto region

The main features of the study variables, from the perspective of the temporal and spatial profiles, arise that ET_0, T_M and T_m exhibit increasing values in spring and summer periods, reaching the greatest mean values in June, for ET_0, and in July for maximum and minimum air temperature; on the other hand, H_M and H_m show an opposite behavior. Finally, *WS* and *R* exhibit high variability and extreme values, especially during the winter period.

In Table 2 some descriptive statistics are listed: it is evident a very high variability, with respect to the corresponding mean value, exhibited by *WS* and *R*, whose values ranging, respectively, from 0 to 11.3 *m/s* and from 0 to 658.2 *mm*, with coefficients of variation equal to 56.408% and 151.611%, respectively. Moreover, the *R* weekly measurements are characterized by a highly right-skewed distribution, with a large proportion (62%) of the recorded values lower than the mean (21.726 *mm*), while the remaining measurements are spread out till the maximum *R* value (658.2 *mm*). Hence, the logarithmic transformation of the *R* values (after adding 1) has been considered and the transformed data have been used in the subsequent analysis. Note that neither ST-BSS nor ST-LCM make distributional assumptions, however transformation towards symmetry is mainly beneficial in a subsequent prediction step based on kriging. As previously pointed out, each variable is featured by a periodic component which has been computed through the weekly averages; then, the recorded data, and the logarithmic values of the *R* measurements, have been deseasonalized by removing the weekly averages. The preprocessed dataset is made available in the R package **SpaceTimeBSS** (Muehlmann et al. 2023) as the dataset **meteo_veneto**.

Table 2 Descriptive statistics of the study variables' measurements*

	Minimum	Median	Mean	Maximum	SD
ET_0	0.086	1.771	2.097	6.657	1.494
	(−1.646)	(2.144)	(2.108)	(6.647)	(0.538)
T_M	−11.286	15.529	15.958	38.300	9.029
	(−7.625)	(16.841)	(16.041)	(41.023)	(4.690)
T_m	−25.420	6.357	6.314	26.800	7.688
	(−17.679)	(7.112)	(6.391)	(25.616)	(4.364)
H_M	0.000	96.143	93.271	100.000	8.247
	(4.830)	(95.395)	(93.302)	(114.550)	(7.524)
H_m	0.000	50.286	52.276	100.000	15.465
	(−10.728)	(52.052)	(52.292)	(113.689)	(12.453)
WS	0.000	1.171	1.303	11.300	0.735
	(−0.051)	(1.155)	(1.302)	(10.967)	(0.708)
R	0.000	9.400	21.726	658.200	32.939
	(−1.221)	(2.244)	(2.121)	(6.877)	(1.461)

*in brackets the statistics of the deseasonalized variables; for the *R* variable, the statistics in brackets refer to the log-transformed deseasonalized values

The descriptive statistics computed for the deseasonalized values and listed in Table 2 (values in brackets) have highlighted very different magnitudes for the data at hand, hence a standardization procedure has been applied and scaled variables with zero mean and unit variance have been considered in the next stages of the analysis. While this standardization has no impact on ST-BSS which is affine equivariant it is relevant for ST-LCM which is only orthogonal equivariant and the question of standardization is similar to the one in principal component analysis.

5.1 Identification of the hidden components

In this section the hidden components which characterize the investigated phenomenon will be identified through both the ST-BSS and the ST-LCM approaches, then spatio-temporal covariance models will be properly chosen and fitted to the detected hidden components.

It is important to consider that, from a computational perspective, the functions used in this case study to identify the latent components through the ST-BSS method are available in the R package **SpaceTimeBSS** (Muehlmann et al. 2022); on the other hand, the R functions adopted for the ST-LCM approach are available on request from the authors.

5.1.1 ST-BSS approach

By recalling the ST-BSS workflow outlined in Sect. 2, the first step of this modeling approach concerns the estimation of the unmixing matrix.

In this case study, stSOBI method (Sect. 2.2) has been applied and the spatio-temporal kernels have been chosen to consider the spatio-temporal dependence. In particular, fifteen kernels have been considered:

- three ball kernels with radius equal to 1, 2 and 3 weeks for the temporal part,
- three ball kernels with radius equal to 30 km, 60 km and 90 km, for the spatial part,
- nine ring kernels with temporal lags equal to 1, 2 and 3 weeks and spatial lags (0, 30) km, (30, 60) km and (60, 90) km, for the spatio-temporal part.

The choice of the kernel setting has been supported by the evaluation of the temporal lags where the correlation is strong and by some descriptive statistics on the Euclidean distance among the spatial locations.

In Table 3 a summary of the kernels' parameters, as well as the corresponding pseudo-eigenvalues, is provided. These latter values have highlighted the most relevant kernel setting for each latent component. Higher pseudo-eigenvalues for the temporal lags 1, 2 and 3 can be recognized for z_1, z_4,

Table 3 Kernel settings and pseudo-eigenvalues for the 15 kernel functions

Kernel Function	r_s (r_{s_0}, r_{s_1})	r_t	z_1	z_2	z_3	z_4	z_5	z_6	z_7
Ball	0	1	1.17	0.44	0.40	1.02	0.60	1.08	1.07
Ball	0	2	1.07	0.26	0.31	0.90	0.50	1.02	1.02
Ball	0	3	1.06	0.23	0.30	0.88	0.48	1.00	1.01
Ball	30	0	2.21	2.65	1.84	1.14	1.26	0.83	0.71
Ball	60	0	3.24	4.26	2.76	1.67	1.66	0.92	0.86
Ball	90	0	3.34	5.29	3.28	2.03	1.78	0.79	0.77
Ring	(0, 30)	1	2.22	0.94	0.24	0.40	0.31	0.39	0.06
Ring	(0, 30)	2	1.96	0.47	0.07	0.13	0.18	0.33	−0.02
Ring	(0, 30)	3	1.92	0.39	0.05	0.12	0.15	0.31	−0.03
Ring	(30, 60)	1	2.58	1.31	0.26	0.66	0.30	0.33	0.16
Ring	(30, 60)	2	2.23	0.64	0.02	0.28	0.14	0.25	0.06
Ring	(30, 60)	3	2.16	0.54	0.01	0.26	0.10	0.21	0.04
Ring	(60, 90)	1	1.06	1.26	0.21	0.67	0.15	−0.13	−0.17
Ring	(60, 90)	2	0.72	0.61	0.01	0.31	0.02	−0.20	−0.23
Ring	(60, 90)	3	0.65	0.53	−0.01	0.29	−0.01	−0.23	−0.24

Table 4 Unmixing matrix for the seven latent spatio-temporal random fields

	ET_0	T_M	T_m	H_M	H_m	WS	R
z_1	−0.44	1.06	0.17	0.19	0.12	0.30	−0.14
z_2	0.22	−0.88	0.69	0.25	0.27	−0.09	0.48
z_3	−0.85	1.80	−0.94	−0.14	−0.57	0.30	1.03
z_4	2.18	−2.56	1.07	−0.20	−0.04	0.24	0.15
z_5	0.14	−2.19	1.81	1.49	−1.66	0.11	−0.17
z_6	0.04	−1.30	1.70	−0.16	−0.67	−0.79	0.13
z_7	0.49	0.49	−0.67	0.35	−0.04	−0.50	0.25

z_6 and z_7, hence these temporal lags are more important for the above mentioned components than for the other components. Moreover, the spatial lags equal to 30 km, 60 km and 90 km are relevant for all the components. The remaining spatio-temporal lags are always important for the first and the second component. As described in Muehlmann et al. (2023), the results coming from stSOBI, i.e., the pseudo-eigenvalues, as well as the unmixing matrix ($\mathbf{W}$) and the found latent processes ($\mathbf{Z}(\mathbf{s}, t)$), can be exploited for further analysis.

Moreover, as the transformation used is linear, the elements of the unmixing matrix can be interpreted as the weights of each variable in the linear combination. Hence, by looking at the unmixing matrix (Table 4) it is evident that

- z_1 is mostly described by the difference between maximum temperature and evapotranspiration, with a negligible effect of the other meteorological study variables;
- z_2 is characterized by the difference between minimum and maximum temperature and positive contribution of rainfall. Evapotranspiration and humidity (minimum and maximum) produce approximately the same contribution. Moreover, the effect of wind speed is not relevant;
- z_3 is mostly formed by the difference between maximum and minimum temperature in addition to the difference between rainfall and evapotranspiration. Also, a negative contribution of minimum humidity can be recognized;
- z_4 is mostly described by the difference between evapotranspiration and maximum temperature (with opposite signs compared to the first latent component) and minimum temperature;
- z_5 is characterized by the difference between minimum and maximum temperature and the difference between maximum and minimum humidity, while the effect of the other variables is not relevant;
- z_6 is mainly characterized by the difference between minimum and maximum temperature (as already observed for the second and fifth latent components) and negative contribution of minimum humidity and wind velocity;
- z_7 is driven by the difference between maximum and minimum temperature as well as the difference between evapotranspiration and wind speed.

As previously pointed out, the seven latent components are uncorrelated, hence each component has been analyzed

univariately and modeled with the most appropriate spatio-temporal covariance (second step of the ST-BSS approach).

To identify a model for each independent component z_i, $i = 1, \ldots, 7$, it is required to preliminarily estimate the spatio-temporal covariances. The appropriate number of spatio-temporal lags has been defined by considering the points' geometry across the spatio-temporal domain. In particular, 7 lags in space (with a lag spacing of 8 km) and 8 in time (with a lag interval of 1 week) have been fixed, hence $K = 56$ lags in space-time.

In Fig. 2 the 3D plots (left panel) and the corresponding marginals in space and in time (middle panels) for the 7 spatio-temporal sample covariances are provided for each latent component. The sample direct covariance surfaces show a well-structured positive correlation for all lags, a linear behavior at the origin and concave for small lags; finally, a different variability in space and in time is evident.

To select a suitable class of covariance models, the sample non-separability ratios (19) have been computed for each z_i, $i = 1, \ldots, 7$, by using the R package **covatest** (Cappello et al. 2020). From the box plots displayed in Fig. 2 it is clear that the calculated ratios (19) are uniformly smaller than 1 for each latent component.

Hence, the empirical CFs can be fitted by the product-sum model which is uniformly negative non-separable and it is also appropriate for modeling data that exhibit different variability in space with respect to time (De Iaco et al. 2001b). Therefore, the following models have been considered:

$$\begin{aligned} &c_i(\mathbf{h}_s, h_t) \\ &= k_{1_i} C_{s_i}(\mathbf{h}_s) C_{t_i}(h_t) + k_{2_i} C_{s_i}(\mathbf{h}_s) + k_{3_i} C_{t_i}(h_t), \quad i = 1, \ldots, 7, \end{aligned} \tag{20}$$

with $k_{1_i} > 0, k_{2_i} \geq 0, k_{3_i} \geq 0$, exponential covariance models both in space and in time, namely $C_{s_i} = Exp(||\mathbf{h}_s||; a_{s_i})$ and $C_{t_i} = Exp(|h_t|; a_{t_i})$ with spatial and temporal practical ranges, respectively, a_{s_i} and $a_{t_i}, i = 1, \ldots, 7$.

The parameters of the models (20), which have been estimated through the non-linear regression procedure of the SPSS package, are given in Table 5.

The adequacy of the models found out through the ST-BSS method has been evaluated by carrying out a leave-one-out cross-validation procedure for each latent component. Then, by multiplying the matrix of the predicted latent components by the inverse of the unmixing matrix, the variable of interest, in this case the ET_0 variable, has been predicted, which has been successively re-scaled through the corresponding mean and standard deviation values. The final predicted ET_0 values have been obtained by adding the seasonal component previously estimated. Lastly, true and predicted ET_0 values have been compared through the correlation coefficient (r = 0.995), the mean error (ME = -0.005), the mean absolute error (MAE = 0.113) and the root mean square error (RMSE = 0.150). They confirm the goodness of the models detected with the ST-BSS approach.

Fig. 2 Surface of the sample spatio-temporal covariogram (left), box-plots of sample non-separability ratios classified by spatial and temporal lags, and sample marginal spatial and temporal covariances with the corresponding models (middle), surface of space–time covariance model (right), for the latent components a) z_1, b) z_2, c) z_3, d) z_4, e) z_5, f) z_6, g) z_7

As described in Sect. 3, after modeling the latent independent components univariately, a back-transformation of the variable(s) of interest follows (III step), using the found unmixing matrix. This stage of the analysis will be recalled in the section of the paper devoted to the comparison between ST-BSS and ST-LCM, in terms of prediction results.

5.1.2 ST-LCM approach

According to the modeling steps described in Sect. 3.2 for constructing an ST-LCM, the first stage requires the estimation of the sample direct and cross CFs at different spatial and temporal lags. The latter have been chosen as already done to develop an ST-BSS model for the study dataset, namely 7 lags in space (from 0 to 44 km) and 8 lags in time (from 0 to 7 weeks) for a total of $K = 56$ lags. Hence, the sample direct and cross-covariances have been estimated at the 56 spatio-temporal lags, for the 7 deseasonalized and scaled environmental variables. In Fig. 3 the 3D plots of the 7 direct and 21 cross spatio-temporal covariances are given. It is important to observe that all the empirical direct covariance surfaces show a linear pattern for short space-time lags, and a progressive delay for greater lags; on the other hand, looking at the sample cross-covariance between some variables (i.e., $ET_0 - H_M$, $ET_0 - H_m$, $ET_0 - WS$, $ET_0 - R$, $T_M - H_M$, $T_M - H_m$, $T_M - WS$, $T_M - R$, $H_M - WS$ and $H_m - WS$) it is clear that there is a negative linear relationship.

Then, the (7×7) matrices of the direct and cross-covariances estimated at each lag k, with $k = 1, \ldots, 56$, have been jointly diagonalized through a (7×7) orthonormal matrix $\mathbf{\Psi}$, and 56 diagonal matrices $\mathbf{\Lambda}(\mathbf{h}_s, h_t)_k$, $k = 1, \ldots, 56$, have been obtained, as indicated in (12). Successively, by extracting the diagonal entries of these matrices, the estimates of the 7 basic components have been found out. Then, through the visual inspection of the 3D covariance surfaces as well as of the marginals in space and in time, only $L = 3$ components (Fig. 4) have been kept as these components have demonstrated different levels of variability both spatially and temporally.

In particular, the following scales of spatio-temporal variability have been detected

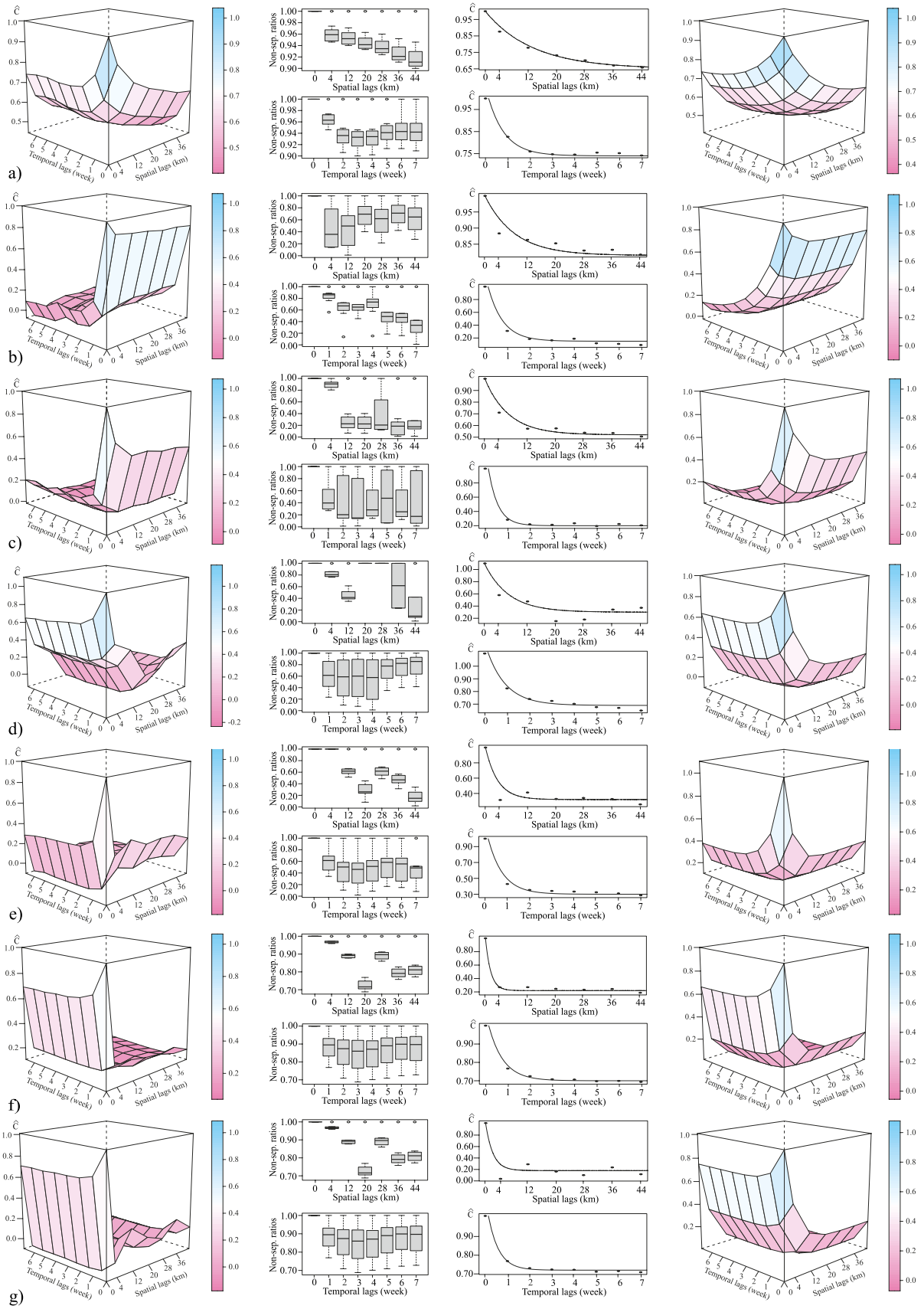
a)
b)
c)
d)
e)
f)
g)
Temporal lags (week)
Spatial lags (km)
Non-sep. ratios

Table 5 Estimates of the models' parameters for the independent components of the ST-BSS model (20)

	z_1	z_2	z_3	z_4	z_5	z_6	z_7
k_1	0.055	0.035	0.280	0.010	0.380	0.080	0.100
k_2	0.495	0.150	0.200	0.690	0.300	0.700	0.720
k_3	0.450	0.815	0.520	0.300	0.320	0.220	0.180
a_s	40 km	25 km	20 km	20 km	10 km	4.5 km	6 km
a_t	2 week	2 week	1 week	3 week	2 week	2 week	1 week

- at 15 km and 1 week (short scale),
- at 18 km and 2 weeks (medium scale),
- at 24 km and 3 weeks (large scale).

Note that the remaining four components have been discarded since their variabilities in space-time were similar to the ones of the chosen components. The second step of the modeling procedure involves finding the most appropriate model classes for the empirical basic covariances. This case study presents statistical evidence supporting the adoption of classes of models which are fully symmetric and non-separable for all the basic components. Moreover, the sample non-separability ratios grouped by spatial and temporal lags, as displayed through the corresponding box-plots in Fig. 4, have been smaller than 1 for all lags, thus uniformly negative non-separable space-time covariance models are the most apt models for the retained latent components (De Iaco et al. 2016; Cappello et al. 2018; De Iaco et al. 2020).

Taking these aspects into account, the product-sum model (De Iaco et al. 2003, 2001a; De Iaco and Posa 2013) has been selected to be fitted to each basic component, i.e.,

$$\begin{aligned} &c_l(\mathbf{h}_s, h_t) \\ &= k_{1_l} C_{s_l}(\mathbf{h}_s) C_{t_l}(h_t) + k_{2_l} C_{s_l}(\mathbf{h}_s) + k_{3_l} C_{t_l}(h_t),\ l = 1, 2, 3, \end{aligned} \tag{21}$$

with $k_{1_l} > 0, k_{2_l} \geq 0, k_{3_l} \geq 0$, C_{s_l} and C_{t_l} the exponential covariance models in space and time, respectively, with practical ranges a_{s_l}, for the former and a_{t_l}, for the latter.

As previously carried out to compute the models' parameters of the ST-BSS independent components, also in this case the parameters' estimation for models in (21) has been computed by performing the non-linear regression procedure available in SPSS. The corresponding values are reported in Table 6.

At this point, the third step of the procedure for the ST-LCM construction concerns the calculation of the coregionalization matrices' elements. In particular, as described in Sect. 3.2, these entries correspond to the ratio between the contributions of the $\widehat{C}_{ij}, i, j = 1, \ldots 7$, at the l-th scale of variability and $[c_l(\mathbf{0}, 0)]$. Hence, by looking at the sample spatio-temporal covariances of the analyzed variables (Fig. 3), and at the spatio-temporal covariance estimates of the 3 basic components (Fig. 4), the elements $b_{ij}^l,\ i, j = 1, \ldots, 7$, $l = 1, 2, 3$, of the coregionalization matrices $\mathbf{B}_l$, have been determined. Finally, the ST-LCM fitted to the matrix-valued CF of the study data, is as follows:

$$\mathbf{C}(\mathbf{h}_s, h_t) = \mathbf{B}_1\, c_1(\mathbf{h}_s, h_t) + \mathbf{B}_2\, c_2(\mathbf{h}_s, h_t) + \mathbf{B}_3\, c_3(\mathbf{h}_s, h_t), \tag{22}$$

where the parameters of the basic covariance models have been specified in Table 6 and $\mathbf{B}_l\ l = 1, 2, 3$, have been as follows:

$$\mathbf{B}_1 = \begin{bmatrix} 1.264 & 0.919 & 0.460 & 0.106 & -0.448 & -0.242 & -0.275 \\ 0.919 & 0.916 & 0.643 & 0.057 & -0.299 & -0.213 & -0.232 \\ 0.460 & 0.643 & 0.829 & -0.081 & 0.069 & 0.011 & 0.012 \\ 0.106 & 0.057 & -0.081 & 1.274 & 0.651 & -0.346 & 0.329 \\ -0.448 & -0.299 & 0.069 & 0.651 & 1.197 & -0.049 & 0.548 \\ -0.242 & -0.213 & 0.011 & -0.346 & -0.049 & 1.510 & 0.076 \\ -0.275 & -0.232 & 0.012 & 0.329 & 0.548 & 0.076 & 1.279 \end{bmatrix},$$

$$\mathbf{B}_2 = \begin{bmatrix} 0.009 & 0.008 & 0.004 & -0.003 & -0.006 & -0.0004 & -0.007 \\ 0.008 & 0.009 & 0.006 & -0.001 & -0.003 & -0.001 & -0.006 \\ 0.004 & 0.006 & 0.008 & 0.002 & 0.004 & -0.001 & -0.001 \\ -0.003 & -0.001 & 0.002 & 0.011 & 0.011 & -0.002 & 0.006 \\ -0.006 & -0.003 & 0.004 & 0.011 & 0.019 & -0.002 & 0.010 \\ -0.0004 & -0.001 & -0.001 & -0.002 & -0.002 & 0.004 & 0.001 \\ -0.007 & -0.006 & -0.001 & 0.006 & 0.010 & 0.001 & 0.016 \end{bmatrix},$$

$$\mathbf{B}_3 = \begin{bmatrix} 3.168 & 3.159 & 1.798 & 0.132 & -1.429 & -0.677 & -1.989 \\ 3.159 & 4.165 & 3.598 & -0.056 & -0.711 & -0.020 & -1.696 \\ 1.798 & 3.598 & 4.837 & -0.208 & 1.023 & 1.032 & -0.295 \\ 0.132 & -0.056 & -0.208 & 3.922 & 2.704 & -1.100 & 1.534 \\ -1.429 & -0.711 & 1.023 & 2.704 & 4.362 & -0.260 & 2.756 \\ -0.677 & -0.020 & 1.032 & -1.100 & -0.260 & 2.141 & 0.369 \\ -1.989 & -1.696 & -0.295 & 1.534 & 2.756 & 0.369 & 4.812 \end{bmatrix}.$$

Note that, the positive definiteness condition of the coregionalization matrices has been checked through the spectral decomposition of the matrices. The condition has been satisfied since, for each $\mathbf{B}_l$, the entries of the eigenvalues' diagonal matrix have been all non negative.

Analogous to evaluating the ST-BSS model's adequacy, the appropriateness of the ST-LCM in (22) has been assessed by the findings from the leave-one-out cross-validation procedure carried out for the primary variable (ET_0). In particular, at each point of the study area, the ET_0 standardized value has been first estimated on the basis of the model in (22) and the values available for all the variables in a properly defined neighborhood; then, the estimated value has been re-scaled by the corresponding mean and standard deviation computed for the ET_0 variable and lastly the ET_0 seasonal component has been added to the re-scaled estimated value. Finally, for the validation of the constructed

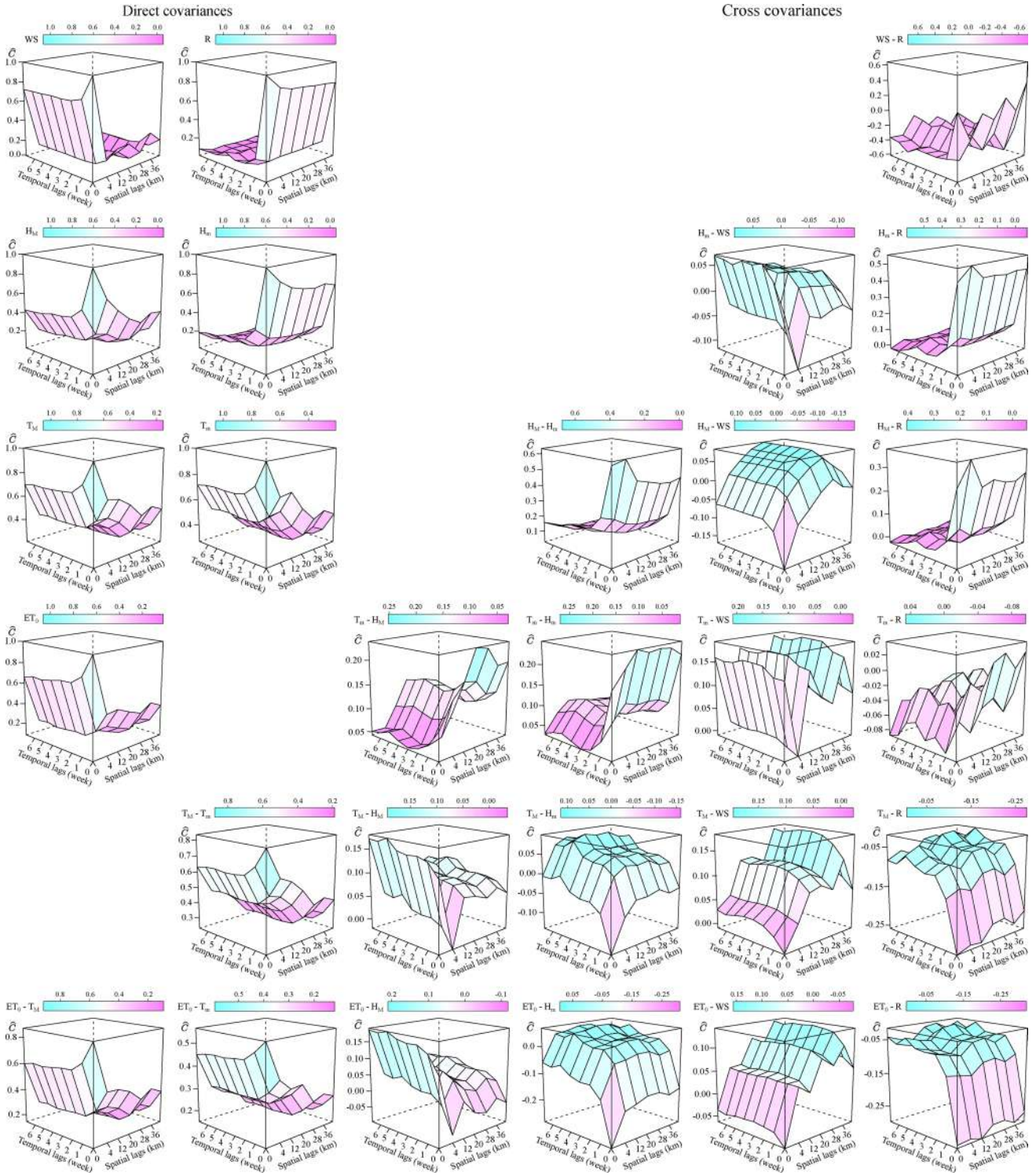

Fig. 3 Surface of the sample spatio-temporal direct and cross covariograms

ST-LCM, the correlation coefficient (r = 0.997), the mean error (ME = 0.002), the mean absolute error (MAE = 0.081) and the root mean square error (RMSE = 0.124) have been computed between the recorded ET_0 values and the estimated ones obtained as stated above. They have highlighted a satisfying adequacy of the model in (22) to describe direct and cross-correlation in space-time between the variables.

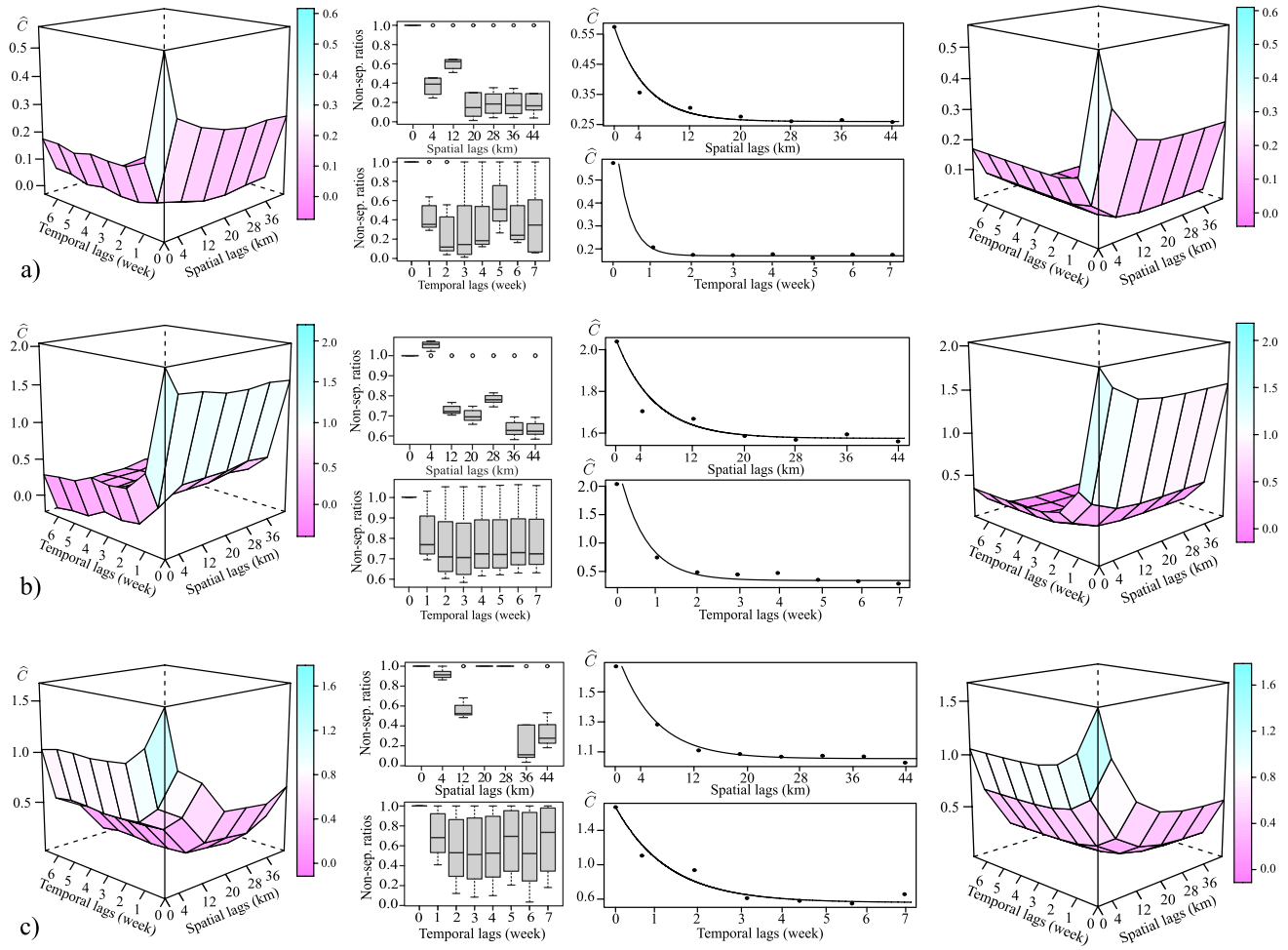

Fig. 4 Surface of the sample spatio-temporal covariogram (left), boxplots of sample non-separability ratios classified by spatial and temporal lags and sample marginal spatial and temporal covariances with the corresponding models (middle), surface of space–time covariance model (right), for the selected basic components at a) short, b) medium and c) large scale of variability

Table 6 Estimates of the models' parameters for the basic components of the ST-LCM (21)

	$l=1$	$l=2$	$l=3$		$l=1$	$l=2$	$l=3$
k_1	0.140	0.125	0.055	a_s	15 km	18 km	24 km
k_2	0.170	0.340	1.055	a_t	1 week	2 week	3 week
k_3	0.260	1.575	0.560				

5.2 Comparison between the two fitted models

In this section the two distinct modeling approaches discussed in the present paper have been compared in terms of predictive performances. In particular, the ST-BSS model and the ST-LCM have been used to compute jack-knife predictions of ET_0 levels for

a) 4 weeks in 2022 after the last observed week, over the 72 sampled spatial locations;
b) 3 weeks in 2020, namely 26th, 43rd and 52nd weeks (belonging to different seasons of the year), over 29 monitoring stations not included in the modeling stage.

Hence, in the case of the ST-BSS model, kriging predictions for all the 7 independent components have been computed first; then by multiplying the predictions' matrix with the inverse of the unmixing matrix, the predictions of the scaled values for all the analyzed variables have been obtained. Successively, the data predicted for the ET_0 variable have been transformed to the scale of the original data, by multiplying them by the corresponding standard deviation and

Table 7 Statistics on the prediction errors of ST-BSS and ST-LCM for ET_0 estimated values for 4 weeks in 2022 at all sampled locations

	+1 week	+2 weeks	+3 weeks	+4 weeks
	ST-BSS predictions			
MAE	0.120	0.101	0.094	0.100
RMSE	0.144	0.125	0.117	0.126
r−MAE	0.045	0.041	0.038	0.038
r−RMSE	0.053	0.049	0.046	0.046
	ST-LCM predictions			
MAE	0.094	0.084	0.092	0.113
RMSE	0.114	0.102	0.113	0.143
r−MAE	0.035	0.034	0.037	0.043
r−RMSE	0.042	0.040	0.044	0.053
$\Delta(\%)$				
MAE	28.46	19.60	2.46	−11.22
RMSE	26.66	22.16	3.87	−12.14

Table 8 Statistics on the prediction errors of ST-BSS and ST-LCM for ET_0 estimated values for 3 weeks in 2020 at 29 testing locations

	2020, 26th week	2020, 43rd week	2020, 52nd week
	ST-BSS predictions		
MAE	0.260	0.153	0.110
RMSE	0.318	0.195	0.137
r−MAE	0.057	0.133	0.279
r−RMSE	0.069	0.168	0.344
	ST-LCM predictions		
MAE	0.291	0.135	0.121
RMSE	0.342	0.174	0.144
r−MAE	0.064	0.117	0.305
r−RMSE	0.075	0.151	0.361
$\Delta(\%)$			
MAE	−10.46	13.33	−8.49
RMSE	−7.08	12.07	−4.72

adding the mean value. In this way, the estimates of the ET_0 residuals have been obtained and lastly, the ET_0 seasonal component previously estimated, added to the residuals.

On the other hand, in the case of the ST-LCM, a spatio-temporal cokriging (De Iaco et al. 2010) based on the fitted model (22) has been carried out to estimate the ET_0 scaled residual values and then, after re-scaling them (i.e., multiplying by the standard deviation and adding the mean value for each monitoring station), the ET_0 seasonal factor has been aggregated to the estimated residuals to obtain the ET_0 weekly predicted levels.

The assessment of the predictive performances concerning the two modeling approaches (ST-BSS versus ST-LCM) has been carried out through four different indicators of the prediction error, namely the mean absolute error (MAE), the root mean square error (RMSE), the relative mean absolute error (r−MAE) and the relative root mean square error (r−RMSE), which have been calculated between the true ET_0 values and the estimated ones. Then, for each error indicator, a percentage relative variation (Δ) between the ST-BSS error indicator and the ST-LCM one (relative to the latter) has been computed to highlight the discrepancy, in terms of predictive performances, between the two approaches. Indeed, a positive (negative) value of Δ indicates an improvement (worsening) in predicting by using the ST-LCM instead of the one based on ST-BSS.

Tables 7 and 8 report the values of the error indicators with the corresponding relative variations concerning, respectively, case a) and case b) previously introduced as two different ways to examine the effectiveness of the two methods. Moreover, in Table 7 the above errors are reported by considering the ST-BSS and the ST-LCM predictions of the ET_0 levels at all sample locations for one, two, three and four weeks in 2022 after the last time available in the study dataset.

From the listed results it is evident that up to 3 time points ahead (weeks), the discrepancies between the true ET_0 values and the predicted ones based on the fitted ST-LCM are lower than the predictions obtained through the ST-BSS approach. The opposite results occurred in the case of predictions at 4 times ahead: in this case the error indicators have highlighted that the ST-BSS approach has improved the ET_0 predictions with respect to the ones resulting on the basis of the ST-LCM. Evidently, the worsening of the predictive performances for the ST-LCM is consistent with the main features of the fitted model (22) which has been defined by considering three different basic components where the largest one referred to a temporal variability equal to 3 weeks.

However, it emerges that, in general, the two compared approaches (ST-BSS versus ST-LCM) have shown a slight difference in terms of predictive performances, with relative variations ranging from -12.14% to 28.46%.

The slight discrepancy between the two adopted procedures to predict ET_0 values, has been also found out in the case b) when the study variable has been estimated for 3 different weeks of 2020, at 29 stations not included in the modeling stage. In this case, the relative variations $(\Delta\%)$ between the error indicators have shown low values, which have been negative (the ST-BSS performed better than ST-LCM) at the 26th and 52nd weeks of 2020, and positive (the ST-LCM performed better than ST-BSS) at the 43rd week of 2020 (Table 8).

Moreover, by looking at the spatial distributions of the percentage relative differences between the ET_0 estimates, computed, alternatively, on the basis of the ST-BSS and the ST-LCM, and the ET_0 true values (Fig. 5), it is evident that, for the three study weeks, the minimum and maximum relative difference occurred at the same locations or at nearby locations.

A further consideration emerging from the maps shown in Fig. 5 is that, for each investigated week, the percentage

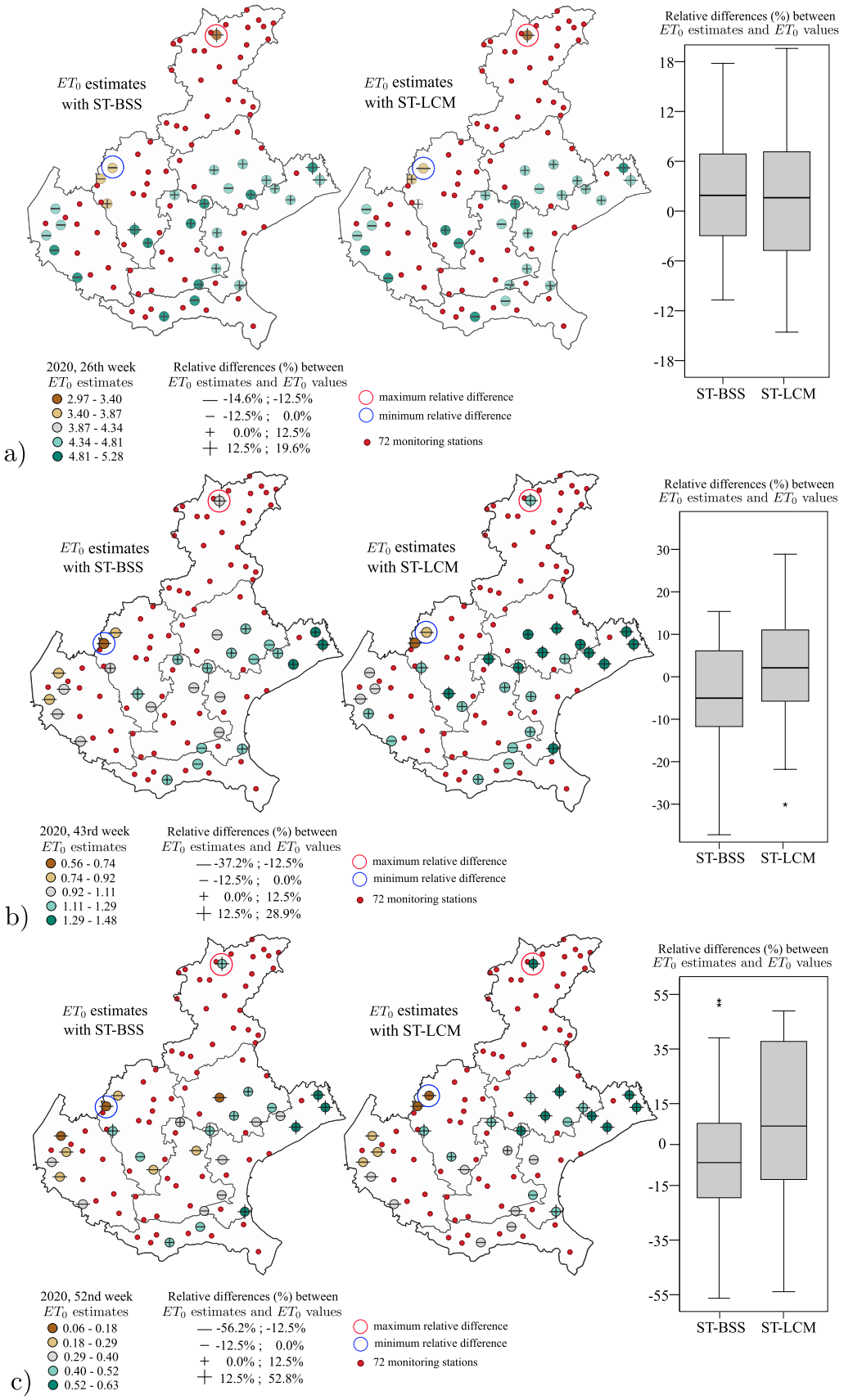

Fig. 5 Estimation maps at 29 stations and box-plots of the relative differences between true ET_0 values versus estimated ones for (**a**) the 26th, (**b**) the 43rd, (**c**) the 52nd week of 2020

Table 9 Parameters for the spatial and temporal CFs of the product-sum covariance model used for simulating multivariate datasets of 3 variables, with 2 or 3 scales of variability

Scales	ST-LCM	ST-BSS	ν	a	ϕ	k_1	k_2	k_3
	(2 scales)	(3 scales)						
1	✓	✓	1.30	1.90	0.80	2/8	1/8	5/8
2		✓	1.00	1.40	0.60	5/8	1/8	2/8
3	✓	✓	0.70	0.90	0.40	5/8	2/8	1/8

Table 10 Parameters for the spatial and temporal covariance models of the product-sum covariance used for simulating multivariate datasets of 7 variables, with 3 or 7 scales of variability

Scales	ST-LCM	ST-BSS	ν	a	ϕ	k_1	k_2	k_3
	(3 scales)	(7 scales)						
1		✓	1.60	2.40	0.90	1/8	2/8	5/8
2		✓	1.45	2.15	0.80	2/8	5/8	1/8
3	✓	✓	1.30	1.90	0.80	2/8	1/8	5/8
4		✓	1.15	1.65	0.70	1/3	1/3	1/3
5	✓	✓	1.00	1.40	0.60	5/8	1/8	2/8
6		✓	0.85	1.15	0.50	1/8	5/8	2/8
7	✓	✓	0.70	0.90	0.40	5/8	2/8	1/8

relative differences between ET_0 estimates and true values have been characterized by the same sign using both the ST-BSS approach and the ST-LCM approach, at almost all locations, namely at 80.5% of the estimated points.

6 Simulation study

Throughout this part of the paper, the predictive ability of the ST-LCM and ST-BSS has been analyzed through a simulation study, based on space-time data, generated over a grid with 64 points in space (irregularly distributed) and 128 points in time. The form of the spatial domains is circumscribed by the square $\mathcal{S}_{n_{sp}} = (0, n_{sp}] \times (0, n_{sp}]$, with $n_{sp} = 8$, from which $n_{sp}^2 = 64$ sample points are selected at random for each simulation iteration; the form of domains in time is of the type $\mathcal{T}_{n_t} = [1, n_t]$, from which the temporal locations are simply $\mathcal{T} \cap \mathbb{Z}$ where $n_t = 128$ equals twice n_{sp}^2 to mimic the unbalanced nature of spatio-temporal datasets that frequently appear in real-world scenarios. Thus, the spatio-temporal coordinates belong to the domains $\mathcal{S}_{n_{sp}} \times \mathcal{T}_{n_t}$ which are denoted hereafter by $[0, n_{sp}]^2 \times n_t$.

The simulations have been performed to produce a total of 120 space-time datasets with

- 3 variables ($p = 3$), in the hypothesis of either 2 scales of variability by using the ST-LCM (I case) or 3 scales of variability by using the ST-BSS (II case);
- 7 variables ($p = 7$), in the hypothesis of either 3 scales of variability by using the ST-LCM (III case) or 7 scales of variability by using the ST-BSS (VI case).

The $(p \times p)$ full-rank coefficient matrix $\mathbf{A}$ of the ST-BSS model, as in (1), as well as the matrices $\mathbf{A}_l$, $l = 1, \ldots, L$, of the ST-LCM, as in (9), have been randomly generated for the different options under study. The latent random fields for both models have been simulated through the product-sum CFs, whose spatial part is modeled with Matérn covariance function, i.e.,

$$C_s(\mathbf{h}_s; \nu, a) = \frac{1}{2^{\nu-1}\,\Gamma(\nu)} \left(\frac{\mathbf{h}_s}{a}\right)^{\nu} \mathcal{K}_\nu \left(\frac{\mathbf{h}_s}{a}\right), \tag{23}$$

where $\nu > 0$ is the smoothness parameter, $a > 0$ is the range parameter and $\mathcal{K}_\nu$ is a modified Bessel function of the second kind with shape parameter ν, while an exponential CF, resulting from an autoregressive temporal process of order 1, is adopted for the temporal part, i.e.,

$$C_t(h_t; \phi) = \phi^{|h_t|}, \tag{24}$$

where $\phi \in (-1, 1)$.

The parameters for the spatial and temporal CFs of the product-sum covariance model used for simulating multivariate datasets of 3 variables, with 2 or 3 scales of variability, and for simulating multivariate datasets of 7 variables, with 3 or 7 scales of variability are given in Tables 9 and 10, respectively.

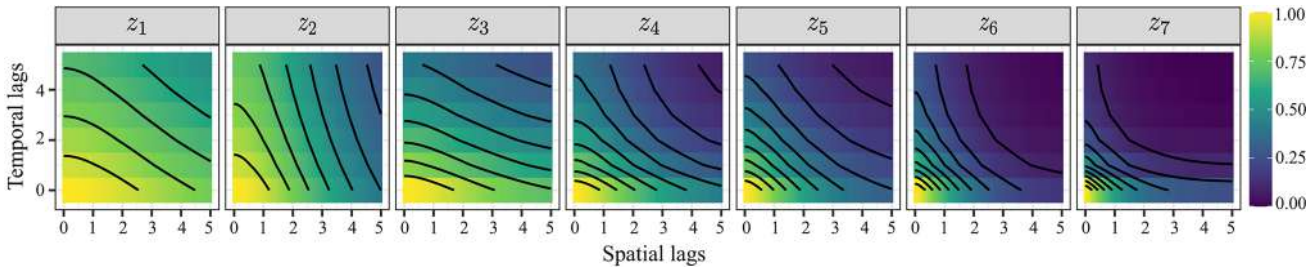

Fig. 6 Surfaces of the product-sum covariance model used for simulating multivariate datasets of 7 variables, with parameters (ν, a, ϕ, k_1, k_2, k_3): (1.60, 2.40, 0.90, 1/8, 2/8, 5/8) for z_1, (1.45, 2.15, 0.80, 2/8, 5/8, 1/8) for z_2 , (1.30, 1.90, 0.80, 2/8, 1/8, 5/8) for z_3, (1.15, 1.65, 0.70, 1/3, 1/3, 1/3) for z_4, (1.00, 1.40, 0.60, 5/8, 1/8, 2/8) for z_5, (0.85, 1.15, 0.50, 1/8, 5/8, 2/8) for z_6, (0.70, 0.90, 0.40, 5/8, 2/8, 1/8) for z_7

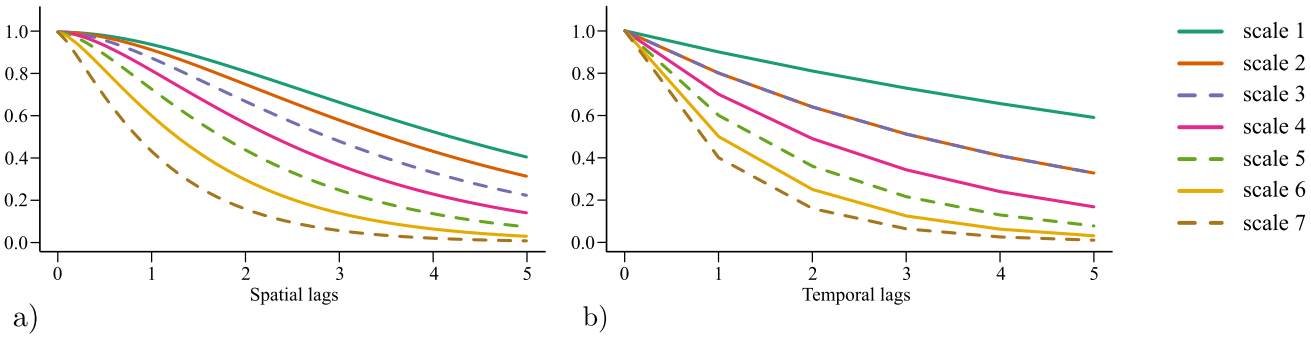

Fig. 7 (**a**) Spatial models with Matérn CF and (**b**) temporal models with exponential CF resulting from an AutoRegressive temporal process of order 1, with 7 variables ($p = 7$) and 3 (dashed lines) or 7 (dashed and solid lines) scales of variability

Moreover, the 7 surfaces of the product-sum CFs in the hypothesis of 7 scales of variability are provided in Fig. 6 and the corresponding spatial part, modeled with the Matérn class model, and temporal part modeled with the autoregressive model of order 1, are given in Fig. 7.

The performance of the two modeling methodologies (ST-LCM and ST-BSS) has been measured by evaluating the absolute and relative deviations, previously defined (Sect. 5.2), between the simulated values and the predicted values in the last three times of the spatio-temporal grid $\mathcal{S}_{n_{sp}} \times \mathcal{T}_{n_t}$.

In particular, both the ST-LCM and ST-BSS have been used to make predictions for each of the 4 options considered in the simulation procedure, that is, simulations for MSTRFs of 3 variables with 2 or 3 scales of variability, based on the ST-LCM and ST-BSS, respectively (I and II cases), and simulations for MSTRFs of 7 variables with 3 or 7 scales of variability, based on the ST-LCM and ST-BSS, respectively (III and IV cases).

In Table 11, the average values of the absolute and relative error indicators (MAE, RMSE, r−MAE, r−RMSE as in Sect. 5.2) related to the 4 simulation options are presented. Note that for each option, the error statistics associated to the ST-BSS and ST-LCM predictions for the first time point ahead, the first 2 time points ahead and 3 time points ahead are specified. Then, the relative variation Δ (in percentage), which measures the relative improvement/worsening (negative/positive sign respectively) of the ST-BSS vs the ST-LCM, has been computed for both the MAE and the RMSE. Moreover, the hypothesis test has been conducted in order to check whether there is no difference between the performance (in terms of mean errors) of the 2 methodologies (δ=0); thus, the T test statistics and the corresponding p-values of the test statistic are also given.

Comparing the errors indexes, in the II and IV cases, the ST-BSS performs slightly better than the ST-LCM and this can be essentially explained by the consideration that the ST-LCM is based on a lower number of latent components (2 or 3, respectively) with respect to the effective number of scales of variability (3 or 7, respectively), thus ST-LCM loses the information related to the neglected latent components at some scale of variability. As highlighted hereafter, note that the difference between the two methodologies is particularly significant in the last case (Fig. 8).

In the I and III cases, the differences between ST-BSS and ST-LCM are smaller, and the p-values are higher than the ones associated with the II and IV cases. In addition, in the case III, the ST-LCM performs better than the ST-BSS method at least up to 2 times ahead, where the correlation is stronger; indeed, the ST-BSS makes forecasts using 7 independent components, of which only 3 can be associated to 3 different scales of variability and then only 3 components can provide a substantial contribution, so ST-BSS forecasts

Table 11 Statistics on the prediction errors of ST-BSS and ST-LCM for 4 simulation cases, differentiated by 1 time ahead, 2 times ahead, 3 times ahead

	I simulation case			II simulation case		
	3 var. 2 scales			3 var. 3 scales		
	+1 t	+2 t	+3 t	+1 t	+2 t	+3 t
	ST-BSS predictions using 3 latent comp.					
MAE	2.342	2.690	2.920	2.551	2.949	3.269
RMSE	2.883	3.306	3.596	2.895	3.464	3.900
r−MAE	0.678	0.735	0.770	0.688	0.751	0.828
r−RMSE	0.681	0.736	0.771	0.665	0.737	0.808
	ST-LCM predictions using 2 latent comp.					
MAE	2.426	2.797	3.099	2.653	3.074	3.477
RMSE	2.966	3.431	3.825	3.027	3.644	4.153
r−MAE	0.706	0.775	0.829	0.720	0.804	0.891
r−RMSE	0.704	0.773	0.830	0.698	0.787	0.878
Δ(%)						
MAE	−3.47	−3.83	−5.78	−3.81	−4.07	−5.97
RMSE	−2.80	−3.65	−5.98	−4.36	−4.96	−7.20
Test δ=0						
Stat. test	−0.277	−0.337	−0.549	−0.330	−0.389	−0.614
p-value	0.783	0.737	0.585	0.743	0.699	0.542
	III simulation case			IV simulation case		
	7 var. 3 scales			7 var. 7 scales		
	+1 t	+2 t	+3 t	+1 t	+2 t	+3 t
	ST-BSS predictions using 7 latent comp.					
MAE	3.307	3.336	3.418	2.492	2.692	2.885
RMSE	3.900	3.995	4.120	2.763	3.095	3.407
r−MAE	0.814	0.834	0.875	0.583	0.564	0.595
r−RMSE	0.805	0.824	0.868	0.570	0.561	0.602
	ST-LCM predictions using 3 latent comp.					
MAE	3.207	3.290	3.528	3.317	3.674	3.992
RMSE	3.815	3.935	4.260	3.943	4.597	5.066
r−MAE	0.796	0.855	0.898	0.693	0.684	0.717
r−RMSE	0.792	0.842	0.893	0.784	0.860	0.927
Δ(%)						
MAE	3.10	1.40	−3.13	−24.88	−26.73	−27.74
RMSE	2.23	1.51	−3.28	−29.93	−32.68	−32.75
Test δ=0						
Stat. test	0.304	0.137	−0.320	−2.202	−2.651	−2.780
p-value	0.762	0.891	0.750	0.032	0.011	0.008

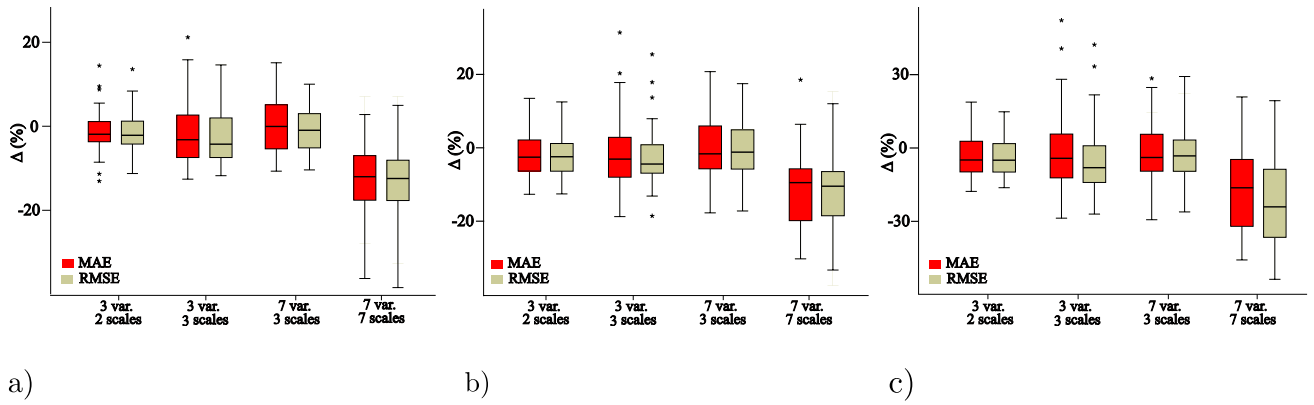

Fig. 8 Box-plot of the relative variations Δ% for predictions based on ST-BSS and ST-LCM at (**a**) 1 time ahead, (**b**) 2 times ahead, (**c**) 3 times ahead

are affected by the noise caused by the non-significant variables.

It is worth noting that the p-values for the I, II and III cases computed distinctly for the 3 intervals of prediction time widely lead to the non-rejection of the null hypothesis at the significance level of 5%, since they range from 0.891 to 0.542. For the last option (IV case), the null hypothesis is not rejected only at a lower level of significance with respect to 5% and this is lower and lower (from 0.032 to 0.008) as the number of time points considered for prediction increases. Thus, there is no significant difference between the performance of the two methodologies. However, these findings might motivate the adoption of the ST-BSS model to produce spatio-temporal predictions, with respect to the ST-LCM when the number of basic components retained by the ST-LCM for prediction is less than 50% of the distinct variability scales, as in case IV; on the other hand, as shown in the case III, the ST-BSS results are affected negatively by the latent components which are involved in the estimate, but are redundant.

7 Conclusions and discussion

In this paper, two different approaches for modeling an MSTRF, namely the widely used ST-LCM and the recently developed ST-BSS method, were discussed and compared in terms of predictive performances. By a thorough presentation of the theoretical features of the two techniques, as well as the main stages of the modeling procedures based on these methods, their similarities and dissimilarities were first highlighted and clarified. Then, both the methodologies based on the ST-BSS and ST-LCM were applied to a dataset concerning seven correlated agrometeorological variables, in order to a) model latent components underlying the multivariate spatio-temporal process at hand, and b) produce spatio-temporal predictions for the variable of interest. The former stage of the application offered the opportunity to point out the different modeling steps occurred in using each of the two methods, while the latter one was carried out to compare the performances of the two methods on the basis of proper prediction error indicators. Finally, a simulation study was also developed to analyze the predictive performances of the two methods.

The parallelism between ST-BSS and ST-LCM, from both the theoretical and the empirical points of view, represents the effective novelty of this contribution. As detailed, although the two methodologies start from different perspectives in modeling an MSTRF, their abilities in predicting the variable of interest over the study domain are mostly equivalent. In both cases, the latent processes are not marginally and spatio-temporally correlated; thus, each process can be analyzed separately in a downstream analysis.

The discussed case study and the analysis developed on the simulated dataset revealed slight differences between ST-BSS and ST-LCM, measured in terms of relative variations between the prediction error indicators. A better performance of ST-LCM with respect to ST-BSS has reasonably arisen when the number of significant latent components is much lower than the number of the original variables, as underlined in the real data application and the simulation study. On the other hand, ST-BSS outperforms ST-LCM, especially in case of a high number of variables, due to the information lost in the ST-LCM fitting process from leaving out some relevant components. The fact that in some cases the two methodologies have a similar performance represents a 'null result' which is defined as an outcome that does not confirm the hypothesis that one method is better than the other.

While both methods seem to work well in practice, there is still some need for future research. BSS approaches, already developed for only spatial and only temporal data, can also handle non-stationary data and this line should also be extended to space-time data (see e.g. Muehlmann et al. 2022, Sipilä et al. 2025). Similarly, here ST-BSS assumes p latent components but usually the hope is that there is room for dimension reduction. In general, there are two main approaches to formulate models with $q < p$ latent components and there are tools to estimate q and the components, like for example Nordhausen et al. (2022) and Muehlmann et al. (2024).

As regards the ST-LCM, future developments can also concern non-stationary and/or spatial anisotropic processes (Muehlmann et al. 2025), as well as, from a computational point of view, a unique user-friendly package for supporting an automatic procedure for all modeling steps, included the number of the relevant latent components to be retained and the class of covariance models to be considered for each latent component.

Funding Open access funding provided by Università del Salento within the CRUI-CARE Agreement. This work was partially supported by the a) European Union-NextGenerationEU with the Cascade Open Calls published by ALMA MATER STUDIORUM - University of Bologna, inside the Project GRINS funded by PNRR - Mission 4, Component 2, Investment 1.3 "Partnership extended to Universities, Research Centers, Firms and research projects funding", D.D. 341 of 15/03/2022, "ECoST-DATA, Exploring Spatio-Temporal Environmental Conditions: Harmonized Databases and Analytical Techniques", CUP: J33C22002910001 b) National Recovery and Resilience Plan (NRRP), Mission 4 Component 2 Investment 1.4 - Call for tender No. 3138 of 16 December 2021, rectified by Decree n.3175 of 18 December 2021 of Italian Ministry of University and Research funded by the European Union-Next GenerationEU. Award Number: Project code CN_00000033, Concession Decree No. 1034 of 17 June 2022 adopted by the Italian Ministry of University and Research, CUP F87G22000290001, Project title "National Biodiversity Future Center

- NBFC" c) HiTEc COST Action (grant CA21163) d) Research Council of Finland (grant 363261)

References

Abulkhair S, Dowd PA, Xu C (2023) Geostatistics in the presence of multivariate complexities: comparison of multi-gaussian transforms. Math Geosci 55(6):713–734

Allard D, Clarotto L, Emery X (2022) Fully nonseparable Gneiting covariance functions for multivariate space–time data. Spatial Stat 52:100706 https://doi.org/10.1016/j.spasta.2022.100706

Babak O, Deutsch CV (2009) An intrinsic model of coregionalization that solves variance inflation in collocated cokriging. Comput Geosci 35(3):603–614

Bachoc F, Genton MG, Nordhausen K, Ruiz-Gazen A, Virta J (2020) Spatial blind source separation. Biometrika 107(3):627–646. https://doi.org/10.1093/biomet/asz079

Berrocal V, Gelfand AE, Holland DM (2010) A bivariate space-time downscaler under space and time misalignment. Ann Appl Stat 4:1942–1975

Bevilacqua M, Hering A, Porcu E (2015) On the flexibility of multivariate covariance models: Comment on the paper by Genton and Kleiber. Stat Sci 30(2): 167–169 https://doi.org/10.1214/15-STS516

Bourotte M, Allard D, Porcu E (2016) A flexible class of non-separable cross-covariance functions for multivariate space–time data. Spatial Stat 18:125–146 https://doi.org/10.1016/j.spasta.2016.02.004

Cabral Pinto F, Manchuk JG, Deutsch CV (2021) Decomposition of multivariate spatial data into latent factors. Comput Geosci 153:104773. https://doi.org/10.1016/j.cageo.2021.104773

Calculli, C., A. Fassò, F. Finazzi, A. Pollice, and A. Turnone (2015) Maximum Likelihood Estimation of the Multivariate Hidden Dynamic Geostatistical Model With Application to Air Quality in Apulia, Italy. Environmetrics 26(2): 406–417. https://doi.org/10.1002/env.2345

Cappello C, De Iaco S, Posa D (2018) Testing the type of non-separability and some classes of space-time covariance function models. Stoch Environ Res Risk Assess 32:17–35. https://doi.org/10.1007/s00477-017-1472-2

Cappello C, De Iaco S, Posa D (2020) Covatest: An R package for selecting a class of space-time covariance functions. J Stat Softw 94(1):1–42. https://doi.org/10.18637/jss.v094.i01

Cappello C, De Iaco S, Palma M, Pellegrino D (2021) Spatio-temporal modeling of an environmental trivariate vector combining air and soil measurements from Ireland. Spat Stat 42 https://doi.org/10.1016/j.spasta.2020.100455

Cappello C, De Iaco S, Palma M (2022) Computational advances for spatio-temporal multivariate environmental models. Comput Stat 37:651–670

Cappello C, Piccolotto N, Muehlmann C, Bögl M, Filzmoser P, Miksch S, Nordhausen K (2024) Visual interactive parameter selection for temporal blind source separation. Journal of Data Science, Statistics, and Visualisation **4**(3). https://doi.org/10.52933/jdssv.v4i3.82

Cardoso JF, Souloumiac A (1996) Jacobi angles for simultaneous diagonalization. SIAM J Matrix Anal Appl 17:161–164

Chen W, Genton MG, Sun Y (2021) Space-time covariance structures and models. Ann Rev Stat Appl 8:191–215

Cichocki A, Amari S (2002) Adaptive Blind Signal and Image Processing: Learning Algorithms and Applications. John Wiley & Sons, New York https://doi.org/10.1002/0470845899

Clarkson DB (1988) Remark AS R74: A least squares version of algorithm AS 211: The F-G diagonalization algorithm. J R Stat Soc C Appl Stat 37(2):317–321. https://doi.org/10.2307/2347359

De Iaco S, Cappello C, Congedi A, Palma M (2023) Multivariate Modeling for Spatio-Temporal Radon Flux Predictions. Entropy 25(7) https://doi.org/10.3390/e25071104

De Iaco S, Cappello C, Palma M, Nordhausen K (2025) A multivariate approach for modeling spatio-temporal agrometeorological variables. Environmetrics 36:e2891. https://doi.org/10.1002/env.2891 https://doi.org/10.1002/env.2891

De Iaco S, Maggio S, Palma M, Posa D (2012) Towards an automatic procedure for modeling multivariate space–time data. Comput Geosci 41: 1–11 https://doi.org/10.1016/j.cageo.2011.08.008

De Iaco S, Posa D (2013) Positive and negative non-separability for space-time covariance models. J Stat Plan Inf 143:378–391. https://doi.org/10.1016/j.jspi.2012.07.006

De Iaco S, Posa D (2018) Strict positive definiteness in geostatistics. Stoch Environ Res Risk Assess 32:577–590

De Iaco S, Myers DE, Posa D (2001a) Space-time analysis using a general product-sum model. Stat Probab Lett 52(1):21–28. https://doi.org/10.1016/S0167-7152(00)00200-5

De Iaco S, Myers DE, Posa D (2001b) Total air pollution and space–time modeling. In:geoENV III, Geostatistics for Environmental Applications, pp. 45–56. P., Allard, D., and Froidevaux, R., eds., Kluwer, Dordrecht, The Netherlands

De Iaco S, Myers DE, Posa D (2003) The linear coregionalization model and the product-sum space-time variogram. Math Geol 35(1):25–38

De Iaco S, Palma M, Posa D (2005) Modeling and prediction of multivariate space-time random fields. Comput Stat Data Anal 48(3):525–547

De Iaco S, Myers DE, Palma M, Posa D (2010) FORTRAN Programs for Space–Time Multivariate Modeling and Prediction. Comput Geosci 36: 636–646. https://doi.org/10.1016/j.cageo.2009.10.004

De Iaco S, Myers DE, Palma M, Posa D (2013) Using simultaneous diagonalization to identify a space-time linear coregionalization model. Math Geosci 45:69–86. https://doi.org/10.1007/s11004-012-9408-3

De Iaco S, Palma M, Posa D (2016) A general procedure for selecting a class of fully symmetric space-time covariance functions. Environmetrics 27:212–224. https://doi.org/10.1002/env.2392

De Iaco S, Palma M, Posa D (2019) Choosing Suitable Linear Coregionalization Models for Spatio-Temporal Data. Stoch Environ Res Risk Assess 33: 1419–1434. https://doi.org/10.1007/s00180-021-01132-0

De Iaco S, Posa D, Cappello C, Maggio S (2019) Isotropy, symmetry, separability and strict positive definiteness for covariance functions: a critical review. Spatial Stat 29:89–108. https://doi.org/10.1007/s00477-017-1472-2

De Iaco S, Posa D, Cappello C, Maggio S (2020) On Some Characteristics of Gaussian Covariance Functions. Int Stat Rev 89: 36–53. https://doi.org/10.1111/insr.12403

Dörr C, Schlather M (2023) Covariance models for multivariate random fields resulting from pseudo cross-variograms. J Multivar Anal 197:105199 https://doi.org/10.1016/j.jmva.2023.105199

Emery X (2010) Interactive algorithms for fitting a linear model of coregionalization. Comput Geosci 36(9):1150–1160

Genton MG, Kleiber W (2015) Cross-covariance functions for multivariate geostatistics. Stat Sci 30(2):147–163. https://doi.org/10.1214/14-STS487

Gneiting T, Kleiber W, Schlather M (2010) Matérn cross-covariance functions for multivariate random fields. J Am Stat Assoc 105(491): 1167–1177 https://doi.org/10.1198/jasa.2010.tm09420

Hyvärinen A, Karhunen J, Oja E (2001) Independent Component Analysis. John Wiley & Sons, New York

Illner K, Miettinen J, Fuchs C, Taskinen S, Nordhausen K, Oja H, Theis FJ (2015) Model selection using limiting distributions of second-order blind source separation algorithms. Signal Process 113:95–103. https://doi.org/10.1016/j.sigpro.2015.01.017

Ip Ryan H.L., Li W.K. (2016) Matérn cross-covariance functions for bivariate spatio-temporal random fields. Spat Stat 17: 22-37. https://doi.org/10.1016/j.spasta.2016.04.004

Ip Ryan, Li W.K. (2017a) A Class of Valid Matérn Cross-Covariance Functions for Multivariate Spatio-Temporal Random Fields. Stat Probabil Lett 130: 115–119 https://doi.org/10.1016/j.spl.2017.07.019

Ip Ryan H.L., Li W.K. (2017b) On Some Matérn Covariance Functions for Spatio-Temporal Random Fields. Stat Sin 27: 805–822 https://doi.org/10.5705/ss.202015.0037

Journel AG, Huijbregts CJ (1978) Mining Geostatistics. Academic Press, London

Jutten C, Taleb A (2000) Source separation: From dusk till dawn. In: Proceedings of the International Symposium on Independent Component Analysis and Blind Signal Separation, pp. 15–26

Krupskii P, Genton MG (2017) Factor copula models for data with spatio-temporal dependence. Spatial Stat 22:180–195

Li B, Genton MG, Sherman M (2007) A nonparametric assessment of properties of space-time covariance functions. J Am Stat Assoc 102:736–744

Miettinen J, Nordhausen K, Oja H, Taskinen S (2012) Statistical properties of a blind source separation estimator for stationary time series. Stat Probab Lett 82(11):1865–1873. https://doi.org/10.1016/j.spl.2012.06.025

Miettinen J, Illner K, Nordhausen K, Oja H, Taskinen S, Theis FJ (2016) Separation of uncorrelated stationary time series using autocovariance matrices. J Time Ser Anal 37(3):337–354. https://doi.org/10.1111/jtsa.12159

Miettinen J, Nordhausen K, Taskinen S (2017) Blind source separation based on joint diagonalization in R: The packages JADE and BSSasymp. J Stat Softw 76(2):1–31. https://doi.org/10.18637/jss.v076.i02

Muehlmann C, Cappello C, De Iaco, S, Nordhausen K (2025) Anisotropic local covariance matrices forspatial blind source separation. AStA Adv Stat Anal. https://doi.org/10.1007/s10182-025-00529-2

Muehlmann C, Nordhausen K, Yi M (2021) On cokriging, neural networks, and spatial blind source separation for multivariate spatial prediction. IEEE Geosci Remote Sens Lett 18(11):1931–1935. https://doi.org/10.1109/LGRS.2020.3011549

Muehlmann C, Bachoc F, Nordhausen K (2022) Blind source separation for non-stationary random fields. Spat Stat 47:100574. https://doi.org/10.1016/j.spasta.2021.100574

Muehlmann C, Filzmoser P, Nordhausen K (2024) Spatial blind source separation in the presence of a drift. Austrian J Stat 53(2):48–68. https://doi.org/10.17713/ajs.v53i2.1668

Muehlmann C, Bachoc F, Nordhausen K, Yi M (2024) Test of the latent dimension of a spatial blind source separation model. Stat Sin 34:1–29. https://doi.org/10.5705/ss.202021.0326

Muehlmann C, De Iaco S, Nordhausen K (2023) Blind recovery of sources for multivariate space-time random fields. Stochastic Environmental Research and Risk Assessment 37, 1593–1613 https://doi.org/10.1007/s00477-022-02348-2

Muehlmann C, Piccolotto N, De Iaco S, Nordhausen K (2022) **SpaceTimeBSS**: Blind Source Separation for Multivariate Spatio-Temporal Data. R package version 0.2-0. 10.32614/CRAN.package.SpaceTimeBSS

Myers DE (1995) The linear coregionalization and simultaneous diagonalization of the variogram matrix function. Sci Terre 32:125–139

Nordhausen K, Oja H (2018) Independent component analysis: A statistical perspective. Wiley Interdiscip Rev Comput Stat 10(5):1440. https://doi.org/10.1002/wics.1440

Nordhausen K, Ruiz-Gazen A (2022) On the usage of joint diagonalization in multivariate statistics. J Multivar Anal 188:104844. https://doi.org/10.1016/j.jmva.2021.104844

Nordhausen K, Virta J (2019) An overview of properties and extensions of FOBI. Knowl Based Syst 173:113–116. https://doi.org/10.1016/j.knosys.2019.02.026

Nordhausen K, Oja H, Filzmoser P, Reimann C (2015) Blind source separation for spatial compositional data. Math Geosci 47(7):753–770. https://doi.org/10.1007/s11004-014-9559-5

Nordhausen K, Taskinen S, Virta J (2022) Signal dimension estimation in BSS models with serial dependence. In: 2022 International Conference on Electrical, Computer, Communications and Mechatronics Engineering (ICECCME), pp. 1–7 https://doi.org/10.1109/ICECCME55909.2022.9988152

Otto P, Fusta Moro A, Rodeschini J, et al. (2024a) Spatiotemporal Modelling of PM2.5 Concentrations in Lombardy (Italy): A Comparative Study. Environ Ecol Stat 31: 245–272. https://doi.org/10.1007/s10651-023-00589-0

Otto P, Fassò A, Maranzano P (2024b) A review of regularised estimation methods and cross-validation in spatiotemporal statistics. Stat Surv 18: 299–340 https://doi.org/10.1214/24-SS150

Pan Y, Matilainen M, Taskinen S, Nordhausen K (2022) A review of second-order blind identification methods. Wiley Interdiscip ReComput Stat 14(4), e1550 https://doi.org/10.1002/wics.1550

Palma M, Maggio S, Cappello C, Congedi A, De Iaco S (2023) Spatio-temporal modeling of groundwater quality deterioration and resource depletion. Hydrogeol J https://doi.org/10.1007/s10040-023-02692-9

Piccolotto N, Bögl M, Gschwandtner T, Muehlmann C, Nordhausen K, Filzmoser P, Miksch S (2022a) TBSSvis: Visual Analytics for Temporal Blind Source Separation. . Vis Inform 6(4) https://doi.org/10.1016/j.visinf.2022.10.002

Piccolotto N, Bögl M, Muehlmann C, Nordhausen K, Filzmoser P, Miksch S (2022b) Visual parameter selection for spatial blind source separation. Computer Graphics Forum 41(3):157–168. https://doi.org/10.1111/cgf.14530

Porcu E, Furrer R, Nychka D (2021) 30 years of space-time covariance functions. Wiley Interdiscip Rev Comput Stat 13(2):1512. https://doi.org/10.1002/wics.1512

Rouhani S, Wackernagel H (1990) Multivariate geostatistical approach to space-time data analysis. Water Resour Res 26:585–591

Sipilä M, Muehlmann C, Nordhausen K, Taskinen S (2024) Robust second-order stationary spatial blind source separation using

generalized sign matrices. Spatial Stat 59:100803. https://doi.org/10.1016/j.spasta.2023.100803

Sipilä M, Cappello C, De Iaco S, Nordhausen K, Taskinen S (2025) Modelling multivariate spatio-temporal data with identifiable variational autoencoders. Neural Netw, 181, 106774 https://doi.org/10.1016/j.neunet.2024.106774

Tang AC, Liu JY, Sutherland MT (2005) Recovery of correlated neuronal sources from EEG: The good and bad ways of using SOBI. Neuroimage 28(2):507–519. https://doi.org/10.1016/j.neuroimage.2005.06.062

Wackernagel H (2003) Multivariate Geostatistics: An Introduction with Applications. Springer, Berlin

Wu B, Guo Y, Kang J (2024) Bayesian spatial blind source separation via the thresholded gaussian process. J Am Stat Assoc 119(545):422–433. https://doi.org/10.1080/01621459.2022.2123336

Xie T, Myers DE (1995) Fitting matrix-valued variogram models by simultaneous diagonalization (part i: Theory). Math Geosci 27:867–876